DEPARTMENT OF THE INTERIOR

U.S. GEOLOGICAL SURVEY

In-Situ Stress Project,

Technical Report Number 6:

Results of Hydraulic Fracturing Stress Measurements at Jianchuan, Western Yunnan Province, China

by

Haimson, B.C.[1], Springer, J.E.[2], Lee, M.Y.[1], Zoback, M.D.[2,3], Li Fangquan[4], Zhai Qingshan[4], and Liang Haiqing[4]

U.S. Geological Survey

Open-File Report 87-477

Prepared in cooperation with the State Seismological Bureau of China, the University of Wisconsin, and Stanford University.

1 University of Wisconsin, Madison, WI

2 U.S.G.S., Menlo Park, CA

3 Stanford University, Stanford, CA

4 Institute of Crustal Dynamics, Beijing, China

1987

CONTENTS

FIGURES

Page

TABLES

RESULTS OF HYDRAULIC FRACTURING STRESS MEASUREMENTS AT JIANCHUAN, WESTERN YUNNAN PROVINCE, CHINA

B.C. Haimson, J.E. Springer, M.Y. Lee, M.D. Zoback, Li Fangquan, Zhai Qingshan, and Liang Haiqing

---

ABSTRACT

Ten hydraulic fracturing stress measurements were performed in an 800 m-deep well at Jianchuan in western Yunnan, China. The minimum horizontal principal stress shows a generally linear increase with depth and the gradient is not as high as that of the theoretical vertical stress calculated from the overburden. Above 450 m most of the Shmin values are greater than or equal to Sv. Below 450 m most of them are less than or equal to Sv, indicating a transition between a thrust and strike-slip stress regime. Assuming a frictional coefficient of between 0.6 and 1.0, the rocks do not appear to be close to failure in either a thrust-faulting or strike-slip mode.

Borehole breakouts were encountered from about 200 m to the bottom of the hole. Their orientations are somewhat scattered at shallow depths and become better defined below 600 m. The average SHmax direction from the breakouts is N15E, which is consistent with the horizontal slip component on major faults in the region. The orientations of six hydraulically induced fractures were determined from impression packers and they are roughly consistent with the breakout directions. The dispersion in breakout and hydraulic fracture orientation is thought to be related to local conditions, such as gravitational loading due to topography.

INTRODUCTION

As part of the Sino-U.S. In-Situ Stress Measurement Project, a series of deep hydraulic fracturing stress measurements were performed in Yunnan Province, China. The measurements were performed in a seismically active region of southwest China (fig. 1), an area that has been selected for intensive studies of the processes related to seismic hazards. The purpose of the project is to understand the contemporary stress field and its relationship to crustal structure and active faulting in the region.

The study area lies in a mountainous area along the east flank of the eastern syntaxial bend of the Himalayan mountain chain. To the west in Burma, the Sagiang fault forms a transform boundary between the Indian and Eurasian plates. The high elevation of the region is a result of the collision between India and Eurasia during the last 30 m.y.

The most prominent tectonic feature in Yunnan is the Red River fault which trends northwest from the Gulf of Tonkin to at least as far as Xiaguan and has a total length of at least 900 km

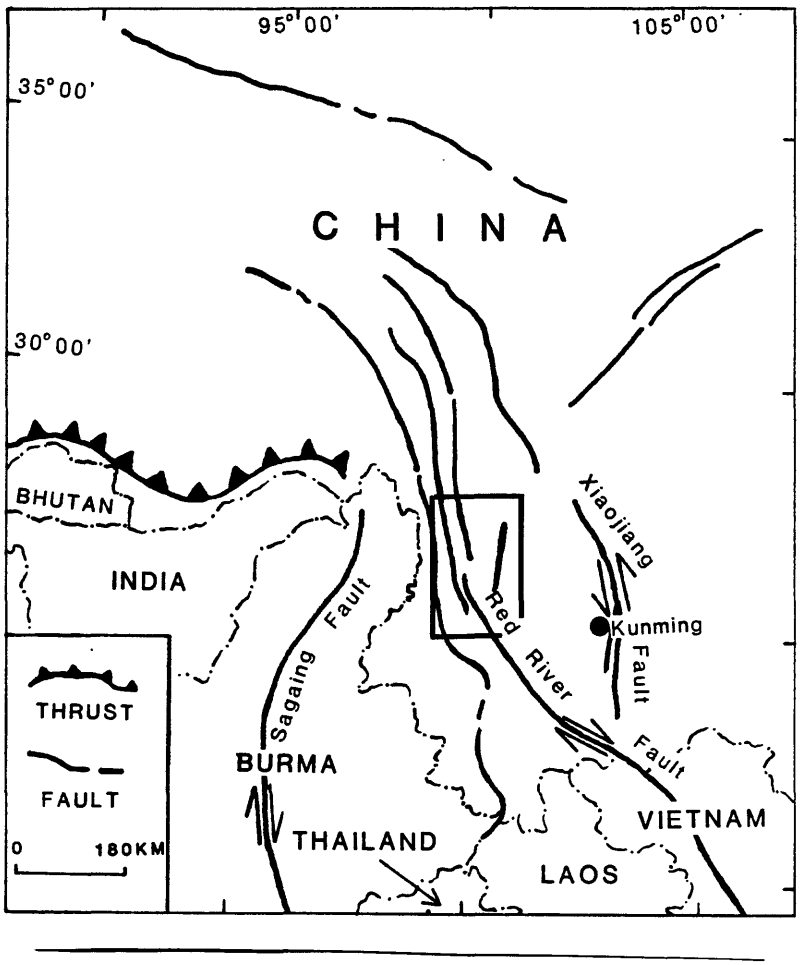

Figure 1. Location map showing the main tectonic features in southwest China. The rectangle represents the area of fig. 2.

(Allen et al., 1984). The dominant sense of slip is right-lateral although some segments have a large normal component. While there have not been any major historic earthquakes along the fault, geologic evidence indicates repeated Holocene movements (Allen, et al., 1984). North of Xiaguan, a series of more northerly trending faults appear to be a continuation of the Red River fault zone, although their sense of motion is said to be predominantly normal (Allen, et al., 1984).

The Xiaojiang fault (fig. 1) is a large left-lateral fault that trends north-south at about 45 degrees to the Red River fault and lies about 50 km east of Kunming. It was associated with two earthquakes of magnitude M 6.5 and M 6.1 in 1985. The Red River fault bends and has a more westerly trend in the region where it is intersected by the Xiaojiang fault.

Earthquake focal mechanisms compiled by Kan et al. (1977) suggest a generally N-S axis of maximum horizontal compression although there is a great deal of scatter in the orientations of the P- and T-axes. In the study area (fig.2), there are two major fault sets. One is N-S to NW-trending and has both right-lateral and normal motion. The other is NNE to NE-trending and has both normal and left-lateral motion. The horizontal component of slip on these faults suggest an average maximum horizontal compression of about N20E (fig. 3).

While the major structures reveal a probable horizontal stress direction, relative magnitudes of the horizontal and vertical stresses remain ambiguous and local variations in the stress field have not been documented. Direct measurements of the magnitude and orientation of the earth's stresses is essential to the understanding the contemporary tectonics and the processes associated with earthquakes. To date, hydraulic fracturing stress measurements have been conducted in two 500 m-deep holes and an 800 m-deep hole. The first two were conducted at Xiaguan and Yongping in 1983 and 1984, respectively. The third set of tests were performed at Jianchuan during 1985 and 1986. This paper describes the geological and geophysical data collected from the Jianchuan test hole as well as the results of the hydraulic fracturing stress measurements.

SITE GEOLOGY

The drill site is located in a narrow, NNE-trending valley 13 km southwest of the city of Jianchuan (fig. 2). It lies midway between the Jianchuan and Lijiang fault zones, which are about 20 km away, although several smaller faults near the site show evidence of recent movement (fig. 4). The relief in the vicinity of the hole is 500 m (fig. 5) and three levels of terraces in the valley suggest 300 m, or more, of late Cenozoic uplift.

The drillhole penetrated 800 m of sandstones and shales of the Eocene Baoshiang Temple Group along with several mica-rich lamprophyre sills of probable Oligocene age. The Baoshiang Temple group is a collection of terrestrial and lacustrine deposits with

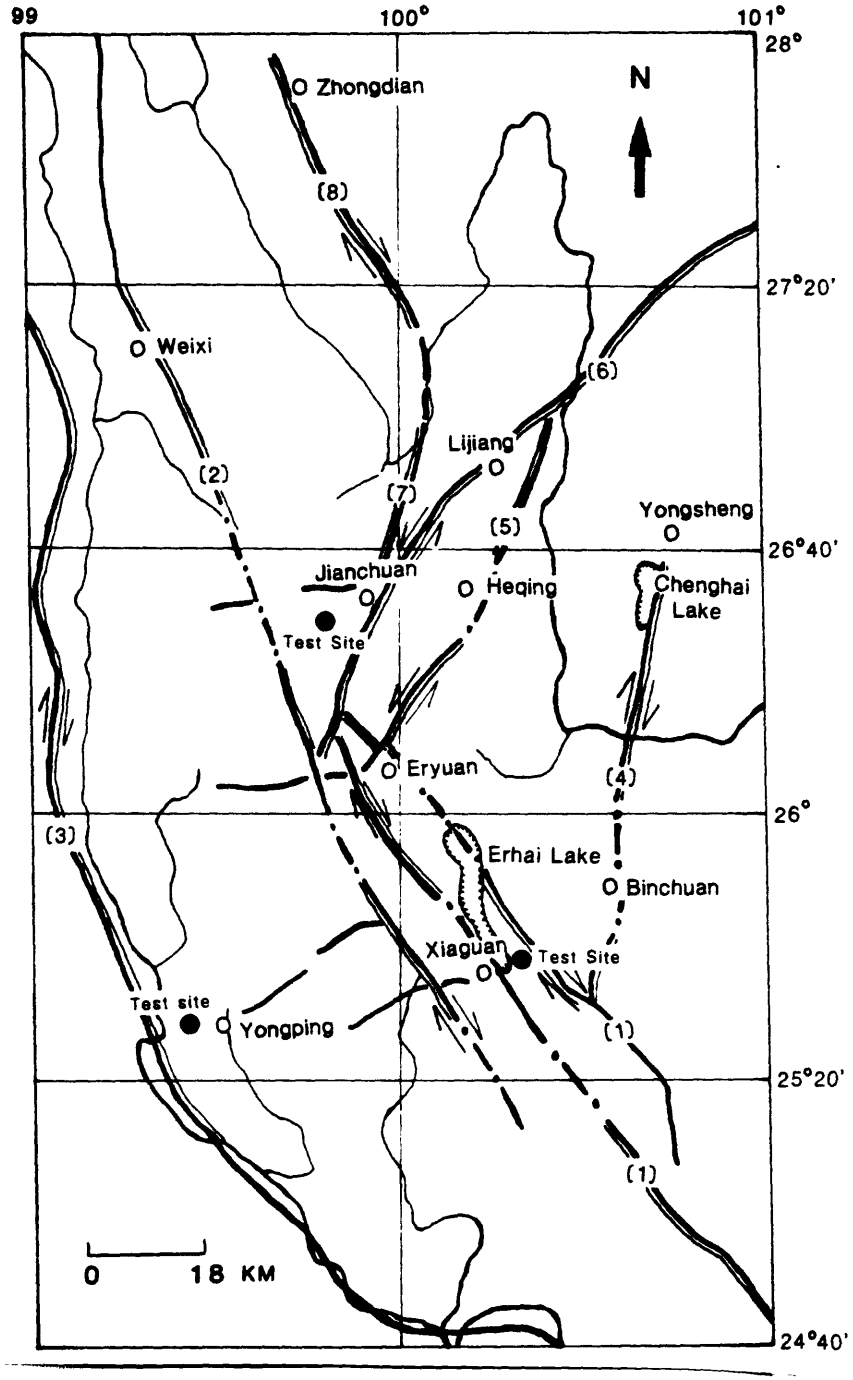

Figure 2. Map showing the main tectonic features of the area and the location of the test wells. Faults keyed by number on the map are: 1: Red River fault, 2: Madeng fault, 3: Lancang River fault, 4: Chenghai-Binchuan fault, 5: Heqing-Eryuan fault, 6:Lijiang fault, 7: Jianchuan fault, and 8: Zhongdian fault. For more information on these faults, see Springer et al. (1987).

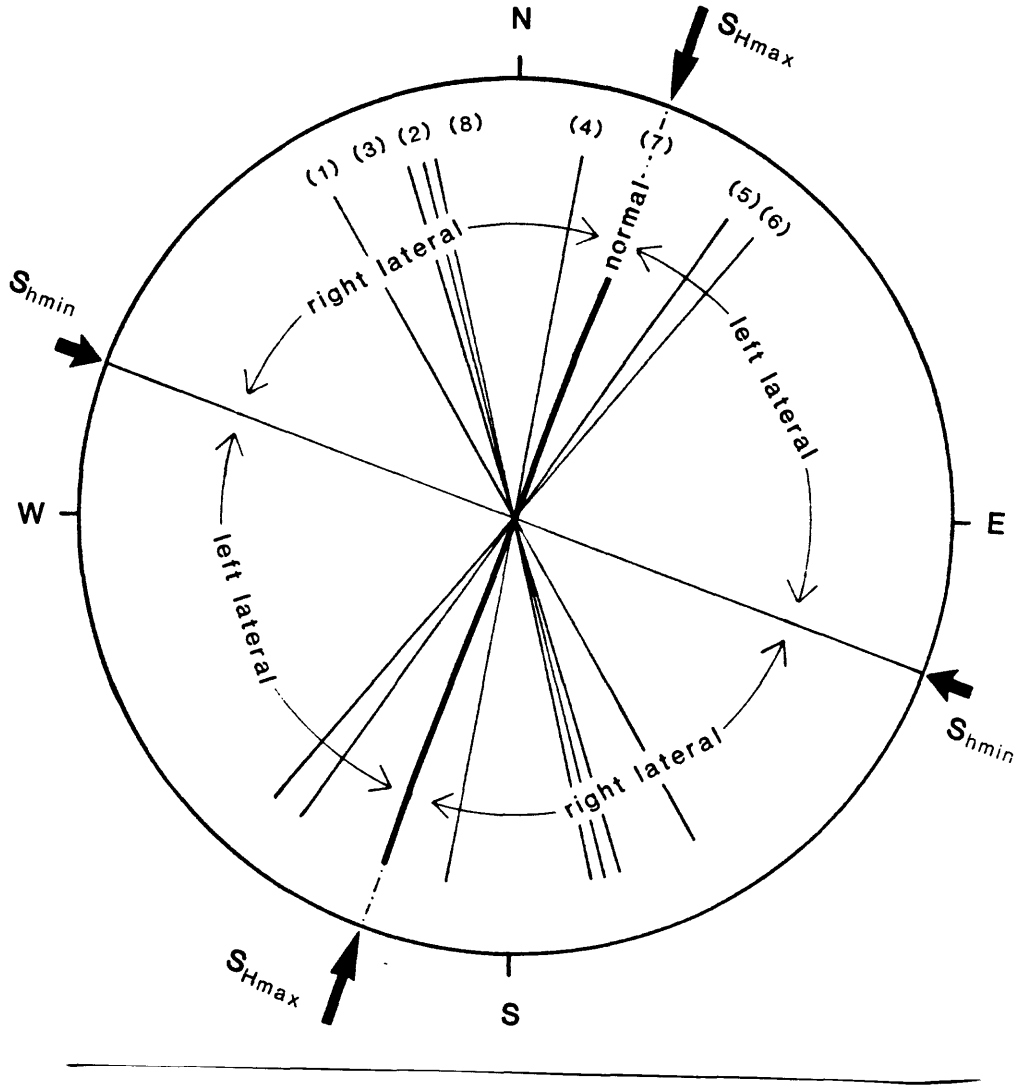

Figure 3. Generalized stress model showing the horizontal principal stress directions and the sense of the horizontal slip component on major faults. Numbers are keyed to the faults in fig. 2.

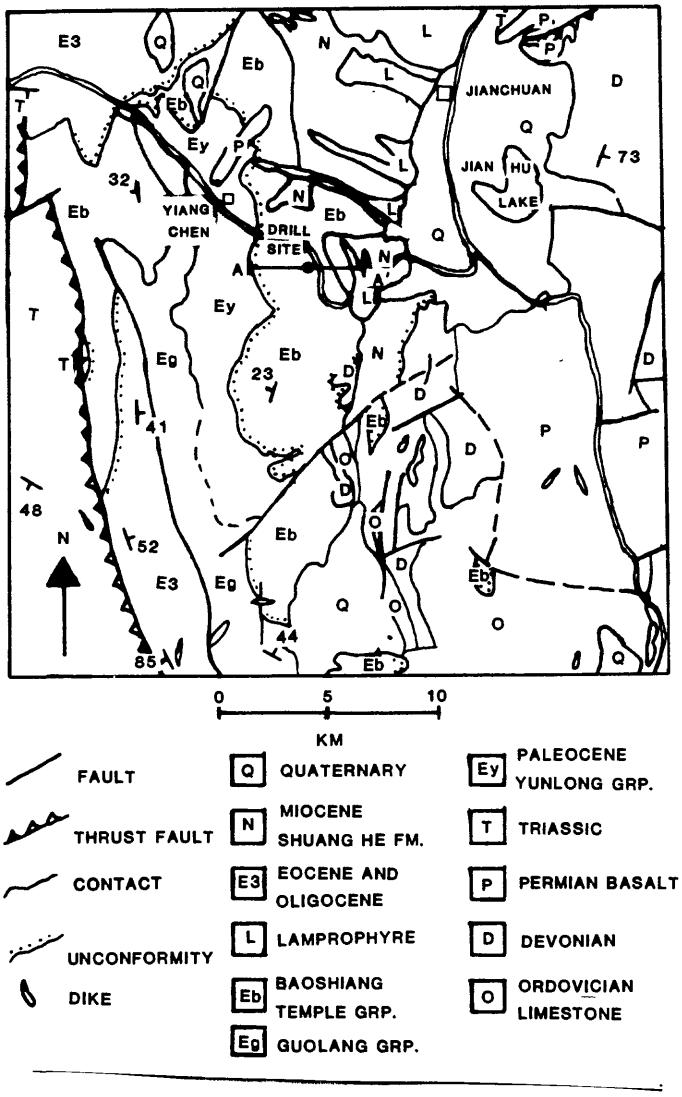

Figure 4. Generalized geologic map of the area around the Jianchuan site. Modified after Geologic Bureau of Yunnan Province (1975).

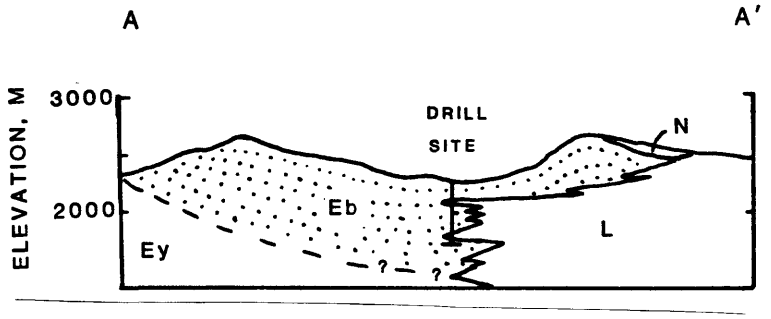

Figure 5. Structure section through the Jianchuan well.

many massive quartz-rich sandstone beds that are competent and homogeneous enough to be quarried by the local population for construction of monuments. In the drillhole, sandstone beds and intrusive sills provided the best intervals for hydraulic fracturing.

The borehole produced a constant flow of water. The main water producing zone lies somewhere between 151 m and 173 m. This is inferred because a packer set at 151 m blocked flow to the surface while a packer set at 173 m allowed the well to continue running.

A borehole televiewer was run in order to determine the distribution and orientations of natural fractures and bedding planes. Analysis of the televiewer logs will be discussed in a later section.

HYDRAULIC FRACTURING STRESS MEASUREMENTS

Method

The hydraulic fracturing method (Hubbert and Willis, 1957) is based on the principle that, in mechanically isotropic rock, a hydraulic fracture will propogate in a plane normal to the least principal stress. Zoback and Zoback (1980) and McGarr and Gay (1978) present data supporting the assumption that, at depth, one principal stress is nearly vertical and the other two are horizontal. Further assumptions made are that the rock is homogeneous, isotropic, and linearly elastic. In a vertical borehole subjected to maximum and minimum horizontal compressive stresses, SHmax and Shmin, respectively, the stress concentrations around the borehole are given by the Kirsch equations (Jaeger and Cook, 1976). Solution of the Kirsch equations indicate that the compressive stresses tangential to the wellbore have a maximum value of 3SHmax - Shmin along the azimuth of Shmin and a minimum of 3Shmin - SHmax along the azimuth of SHmax (fig. 6).

The hydraulic fracturing technique consists of isolating a section of the borehole with inflatable rubber packers and pressurizing the interval between them. As this is done, the the tangential stress along the azimuth of SHmax decreases, becomes negative (tensile) and the rock fractures. The pressure then starts to drop and the well is shut in by a valve at the surface. The pressure at which the rock breaks is called the breakdown pressure Pb.

After the well is shut in, the pressure decays rapidly until the fracture closes, causing a change in the decay rate. The pressure at which the decay rate changes is called the instantaneous shut-in pressure (ISIP). An example of a pressure-time record is shown in fig. 7. Several pressurizing cycles are then performed in order to extend the fracture away from the borehole wall and minimize the effect of stress concentrations near the wellbore. The ISIP is considered to be equal to Shmin.

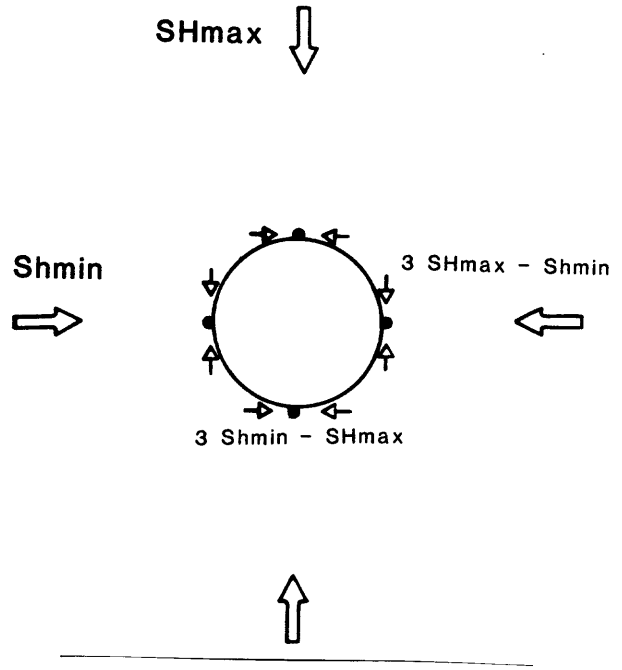

Figure 6. Diagram showing stress concentrations around a borehole.

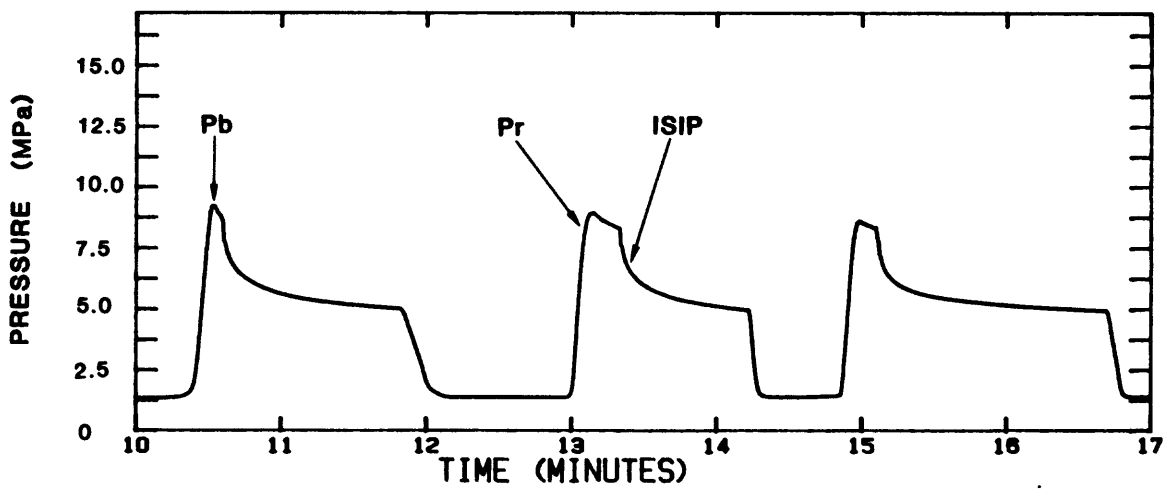

Figure. 7. Example of a pressure-time record.

Viscous pressure loss within the hydraulic fracture may cause the ISIP to be higher on the first cycle. As the fracture propogates, this effect decreases and the shut-in pressure on subsequent cycles approaches Shmin (Hickman and Zoback, 1983).

The maximum horizontal stress is related to the breakdown pressure,Pb by the following relationship derived by Haimson and Fairhurst (1967):

$$Pb = 3Shmin - SHmax - Po + T \qquad [1]$$

where Po is the pore pressure and T is the tensile strength of the rock.

In this report, we use an estimate of the fracture reopening pressure, Pr, to determine SHmax. The fracture reopening pressure is related to SHmax by the following relationship (Bredehoeft et al., 1976):

$$Pr = 3Shmin - SHmax - Po \qquad [2]$$

In other words, the fracture reopening pressure is equivalent to a breakdown pressure when the tensile strength of the rock is zero (fracture is already created).

Fracture opening pressures were estimated from the bend in the pressurization curves. Because the pumping rates were not as constant as we would like, this is only an estimate.

Estimation of the ISIP

Four methods were used to determine the instantaneous shut in pressure. These were the inflection point method (IP), low flow-rate pumping pressure (FL), flow-rate vs pressure (FR), and a non-linear regression method (NLR). The inflection point method is the simplest method and involves chosing an inflection point by inspection of the decay curve. When this inflection point is not apparent, a variation on the method, used successfully by Gronseth and Kry (1983) was employed. To use this method, a straight line, tangent to the decay curve, is drawn from the point of shut in. The pressure at which this line departs from the decay curve is taken as the ISIP (fig. 8).

While pumping on an existing fracture at very low flow-rates, the pressure increase until it reaches a stable plateau. The fracture is barely open at this pressure and the flow rate is just sufficient to keep up with the fluid escaping through the fracture. This estimate of the ISIP is usually a good upper bound.

By plotting the pumping pressure vs flow-rate for several different injection rates, two straight-lines are usually found (fig. 9). The steeper line occurs at pressures in which the fracture is closed and the shallower line occurs when the fracture is open and being extended. The intersection of these two lines is taken as the ISIP. This method is usually more successful when used on a single cycle. The flow rates, however

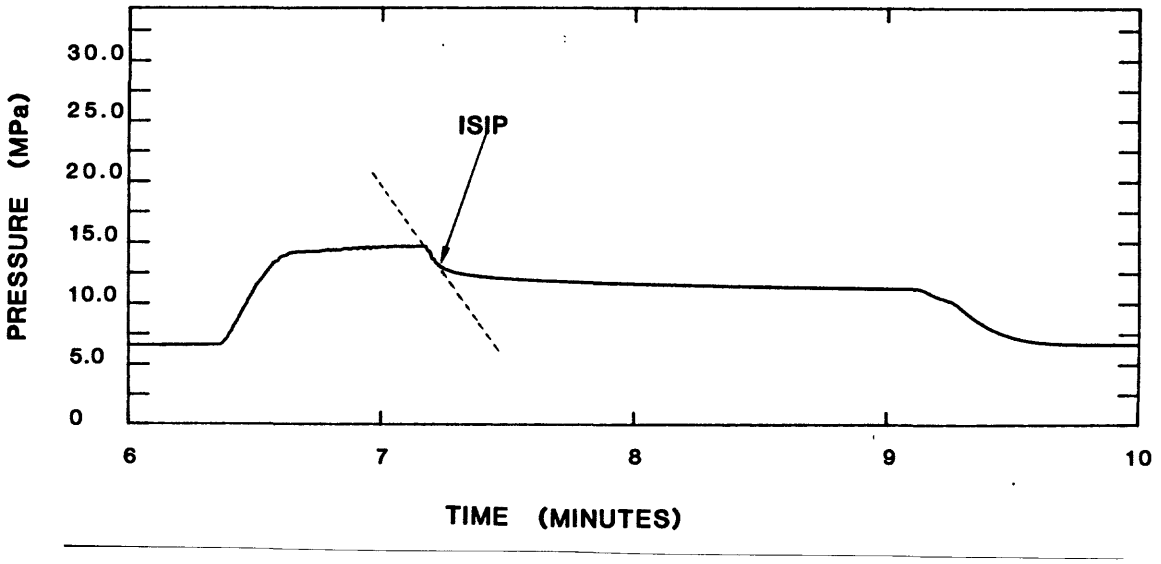

Figure 8. Example of the tangent method for finding the ISIP on a decay curve.

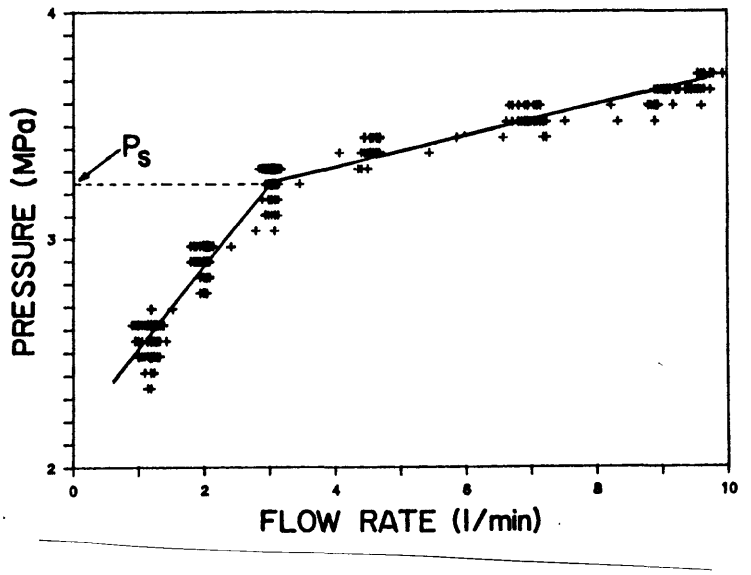

Figure 9. Example of the pressure vs flow-rate method for finding the ISIP (after Haimson and Lee, 1987).

were not always controlledwell enough and we sometimes had to use more than one cycle.

The nonlinear regression method is based on the observation of Muskat (1937) that as fluid flows between a well and porous rock, the pressure decays in a negative exponential fashion. The first segment of the curve does not fit the negative exponential model because the fracture is still open. Assuming that the fracture loses its permeability after it closes, fluid flow into the rock will follow an exponential decay function. A nonlinear regression is run on the digitized pressure-time record from the time the well is shut in. If this regression does not provide a good fit to a negative exponential function, the first point is thrown out and the regression is run on the remaining points. This step is repeated until a negative exponential fit is achieved. The exponential curve is then extrapolated back to the point at which the shut in was initiated and that pressure is taken as the ISIP (Haimson and Lee, 1987).

Hydraulic Fracturing Tests

The hole was drilled with a 130 mm- diameter core barrel to 350 m depth. Between 350 m and 800 m, the hole diameter was 110 mm. In the 130 mm section of the hole, four tests were performed using Lynes inflatable straddle packers with a diameter of 110 mm and an interval length of 2.5 m. Two tests were performed in the 110 mm section using Lynes inflatable packers with a diameter of 100 mm and an interval length of 2.2 m. The four lowest tests were done using a new 100 mm straddle packer developed by the Institute of Crustal Dynamics.

Pressure was applied at the wellhead using a 12-piston Racine pump driven by the diesel engine of a Liaz (Czechoslovakian) truck. Pressure was measured at the surface using a Dynisco 0 to 345 bar (0 to 5,000 psi) transducer and a ZQ-Y type 0 to 250 bar transducer (manufactured in China). The signals from both transducers were recorded in analog form on a LZ3-404 four channel X-Y function (chart) recorder (manufactured in China). The signal from the Dynisco transducer was also recorded on a TI four channel chart recorder. A Flow-Tech flowmeter measured pumping rates at the surface and these data were also output on the two chart recorders.

The signals from the Dynisco transducer and the flowmeter were also digitized in real time by an HP3421A, Data Acquisition/ Control unit, controlled by an HP-85 computer. The data were digitized on two channels at a rate of two readings per second on each channel. The digital records were stored on magnetic tape for further analysis. The first four and the last four tests were digitized. The pressures have been converted to downhole pressure by adding the hydrostatic head. On the flow records, spikes that appear at the end of each cycle are the flow back which has been cycled through the flowmeter. Table 1 summarizes the results from all the tests.

Intervals for all the tests were chosen on the basis of core samples. The borehole televiewer was run after the first four tests were performed.

Table 1

Results of Hydraulic Fracturing Tests
(Stresses in MPa)

Test	Depth (m)	SHmin Min.	SHmin Max.	Shmax Min.	Shmax Max.	Sv	Azimuth of SHmax
A	87	5.8	6.5	--	--	2.3	N63W
B	152	7.3	7.5	7.7	11.9	4.1	N23E
C	174	5.1	5.7	11.7	12.6	4.6	unknown
D	218	6.0	6.4	8.4	9.8	5.9	N35E
E	437	12.4	13.4	19.4	22.9	11.7	N53E
F	451	11.5	12.0	--	--	12.0	--
G	593	14.2	14.3	24.0	25.2	15.8	--
H	668	12.7	13.3	18.0	20.1	17.8	N3W
I	709	15.9	17.7	28.2	32.3	18.9	--
J	751	22.9	24.8	--	--	20.1	N8W

Test A. was performed in the interval from 86 m to 88.5 m with the center at 87.25 m. The rock was a sill that intersected the well from 72.1 m to 93.7 m. A pressure-time record for the test is shown in fig. 10. The initial breakdown pressure was 9.4 MPa. From the inflection point method, the shut-in pressures decreased with successive cycles. The value of 6.0 MPa was chosen from the fourth cycle as representative of Shmin. Using the low flow-rate pumping pressure as an upper bound and comparing the results from the flow-rate vs pressure and nonlinear regression methods, a range of 5.8 to 6.5 MPa was chosen. Televiewer logs (discussed below) indicated that the wellbore had spalled in this interval and the hole was not round. This condition was bad enough that the first attempt to set the packer in this interval resulted in a torn element. These conditions invalidate the assumptions of a round hole in a linear elastic medium, so we did not calculate SHmax. The impression packer revealed a vertical fracture oriented N63W that had not been seen on the pre-fracturing televiewer log.

Test B. was performed in the interval from 150.6 m to 153.1 m

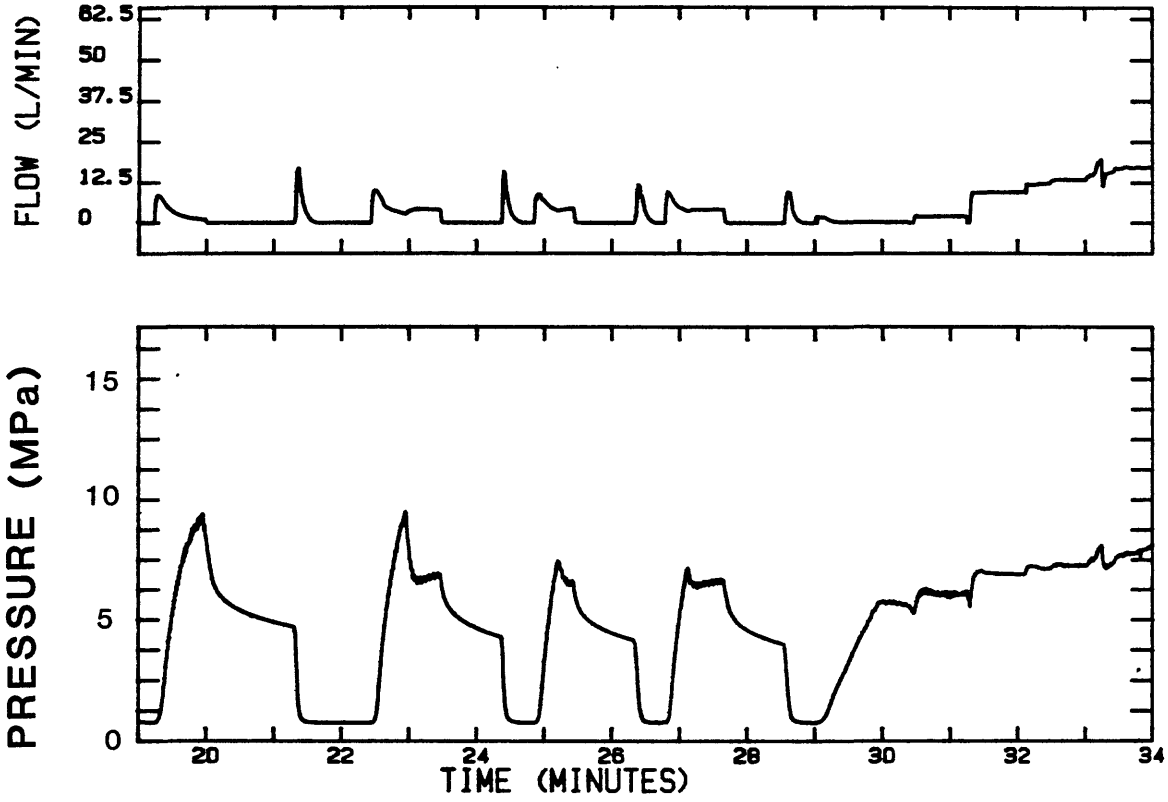

Figure 10. Pressure-time record for the test at 87 m.

with the center at 151.9 m. A pressure-time record for the test is shown in fig. 11. The rock was a very silty sandstone with subhorizontal bedding laminations. None of these, however, appeared to be mechanical breaks. The initial breakdown pressure was 9.4 MPa. The fracture reopening pressures fell in the range from 8.4 to 8.7 MPa (Table 2A). The best shut-in pressure from the third and fourth cycles, using the inflection point method was 7.3 MPa. By using the low flow-rate pumping pressure as an upper bound, a range of 7.3 to 7.5 was chosen for Shmin.

Test C. was run in the interval from 173 m to 175.5 m with the center at 174.25 m. A pressure-time record for the test is shown in fig. 12. The rock was a sill that intersected the well from 166.9 m to 177.7 m. The breakdown pressure was 7.1 MPa and Pr was between 5.5 and 5.8 MPa (Table 2A). Shut-in pressures decreased from one cycle to the next and a value of 5.1 MPa was chosen from the third and fourth cycles using the inflection point method. Using the low flow-rate pumping pressure as an upper bound, a range of 5.1 to 5.7 MPa was chosen for Shmin. The post-fracturing televiewer record showed one horizontal fracture and one high-angle fracture that were not present in the core. The impression packer revealed a vertical fracture, however, the orientation mark was accidentally rotated and the orientation is not known.

Test D. was performed in the interval from 217 m to 219.5 m with the center at 218.25 m. A pressure-time record for the test is shown in fig. 13. The rock was a silty sandstone. The breakdown pressure was 8.3 MPa and Pr was 7.3 to 7.5 MPa. Shut-in pressures

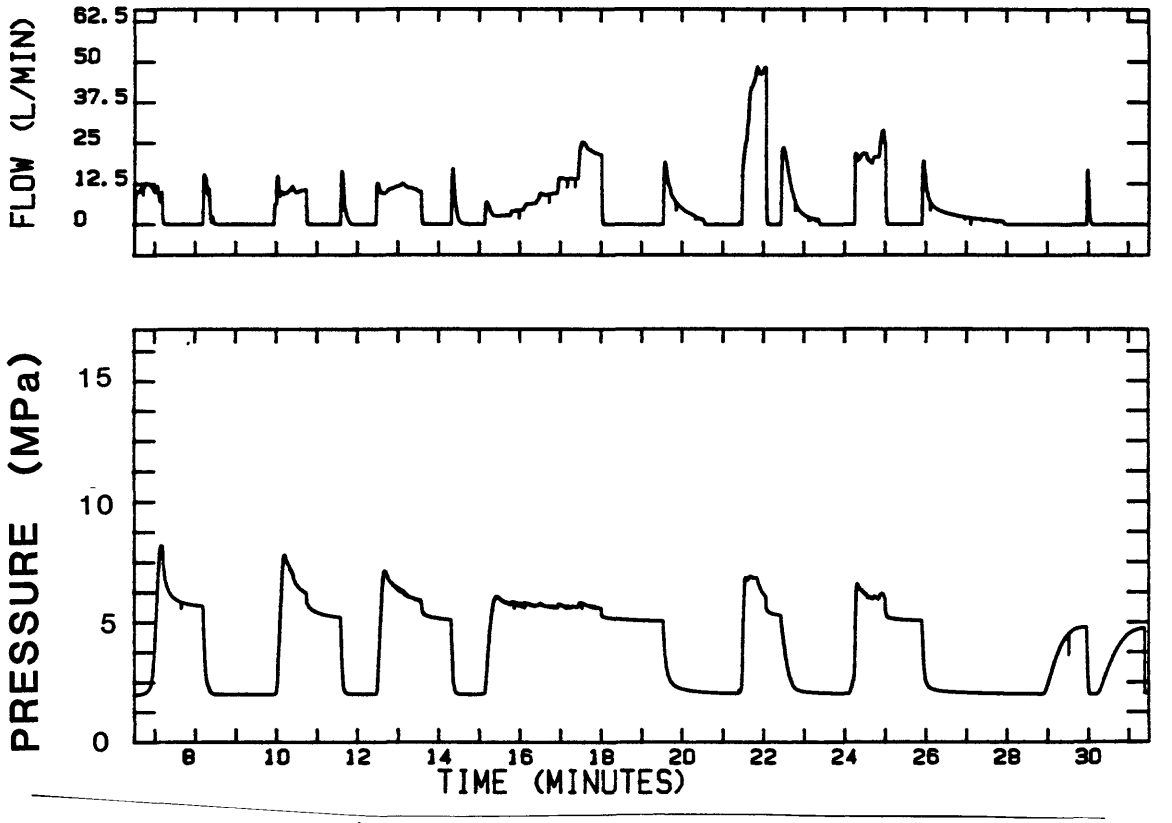

Figure 13. Pressure-time record for the test at 218 m.

decreased from one cycle to the next and, using the inflection point method for cycle 3, the value of 6.3 MPa was chosen. The lowest estimate of the ISIP was 6.0 MPa from the low flow-rate pumping pressure. The highest was 6.4 MPa from the nonlinear regression method. The value of Shmin was therefore 6.0 to 6.4 MPa and the value of SHmax was 8.4 to 9.8 MPa.

The televiewer showed both horizontal and vertical fractures that were not present in the core. The impression packer revealed a previously unseen vertical fracture with a strike of N35E.

Test E. was performed in the interval from 435.9 m to 438.1 m, centered at 437 m. A breakdown pressure of 17.5 MPa was recorded on the first cycle and the fracture reopening pressure was 13.0 to 13.5 MPa. The ISIP's were 12.5, 12.4, and 12.7 MPa using the inflection point, nonlinear regression, and flow-rate vs pressure methods. The upper bound on Shmin was taken from the low flow-rate pumping pressure as 13.4 MPa. Shmin is therefore 12.4 to 13.4 MPa and SHmax is 19.4 to 22.9 MPa. The impression packer revealed a previously unseen vertical fracture with a strike of N53E.

Test F was performed from 449.7 m to 451.9 m, centered in the interval attempted in test number four. The rock was an intrusive that intersected the hole from 435.9 m to 459.2 m. Shut-in pressures were 12.0 MPa from the inflection point method and 11.5 from the low flow-rate pumping pressure. There was no observable breakdown pressure and the fracture reopening pressures were too

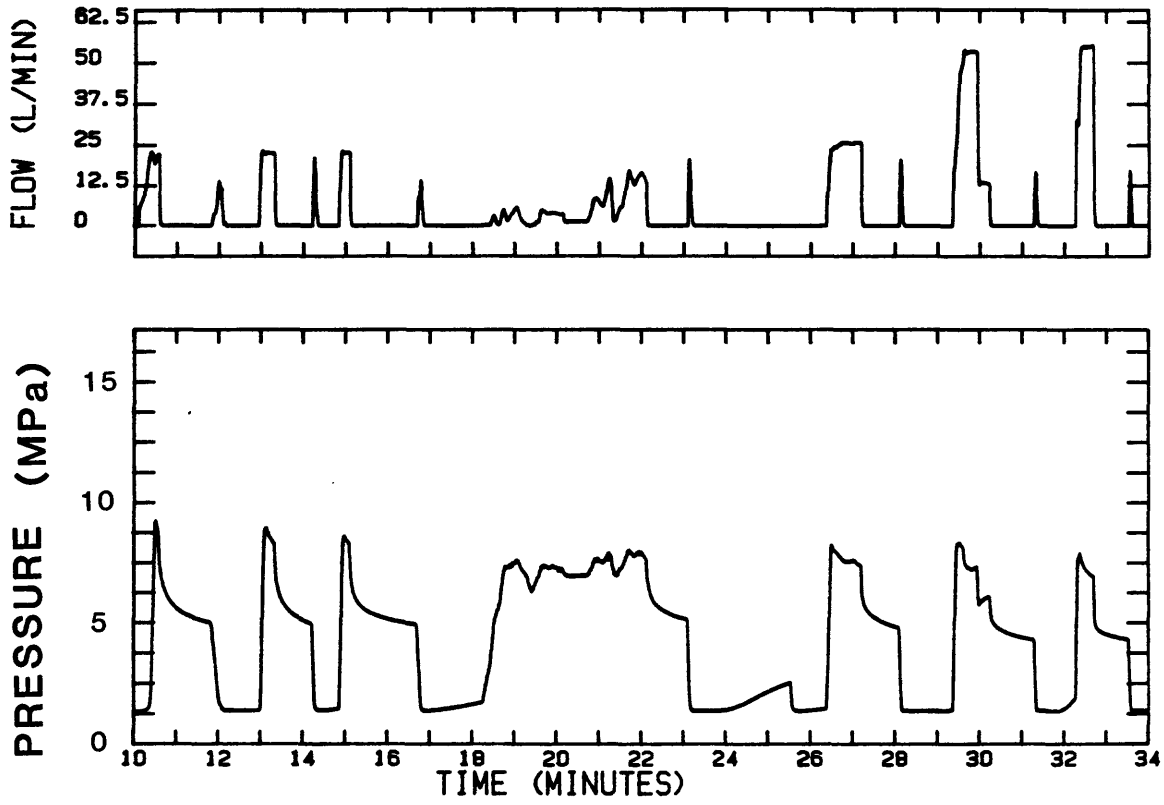

Figure 11. Pressure-time record for the test at 152 m.

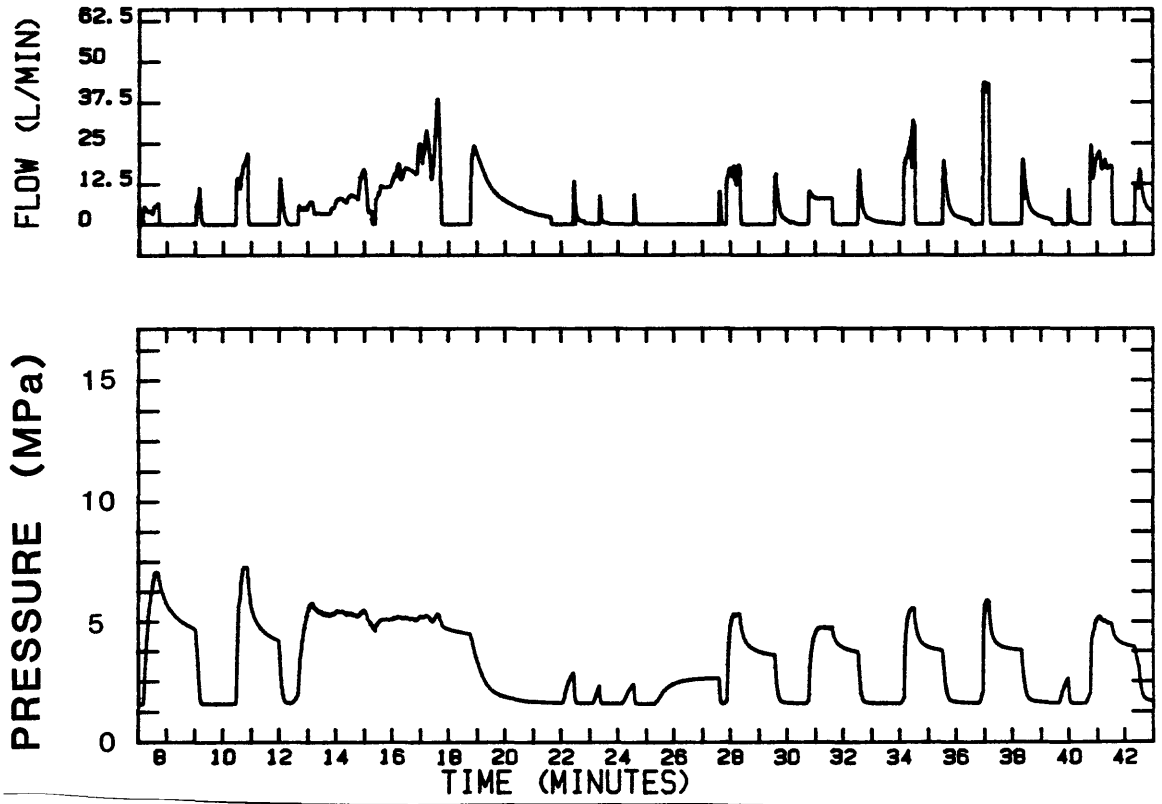

Figure 12. Pressure-time record for the test at 174 m.

ambiguous to use for a determination of SHmax. It appears from the slow pressure increases on these curves, that the pumping rates were not sufficient to overcome fluid loss in the system. High-angle joints intersected the core at either end of the test interval and these joints were possible sources of fluid loss.

Test G was performed in an interval centered in clayey siltstone at 593 m. A pressure-time record for the test is shown in fig. 14. The initial breakdown pressure was 18.3 MPa and Pr was in the range of 11.9 to 12.8 MPa. The best pick for the ISIP from the inflection point method was 14.2 MPa and the best pick from the nonlinear regression method was 14.3 MPa.

Test H was performed at 668 m in fine sandstone. A pressure-time record for the test is shown in fig. 15. Using the inflection point method, the ISIP from the first cycle was chosen as the best pick. The average ISIP from the nonlinear regression method was 12.7 MPa and the upper bound on Shmin was chosen from the low flow-rate pumping pressure of 13.2 MPa. The breakdown pressure was 15.6 MPa and the best picks for Pr were from 13.2 to 13.5 MPa. The estimate of SHmax is therefore 18.0 to 20.1 MPa. The impression packer revealed a high-angle fracture with a strike of N3W.

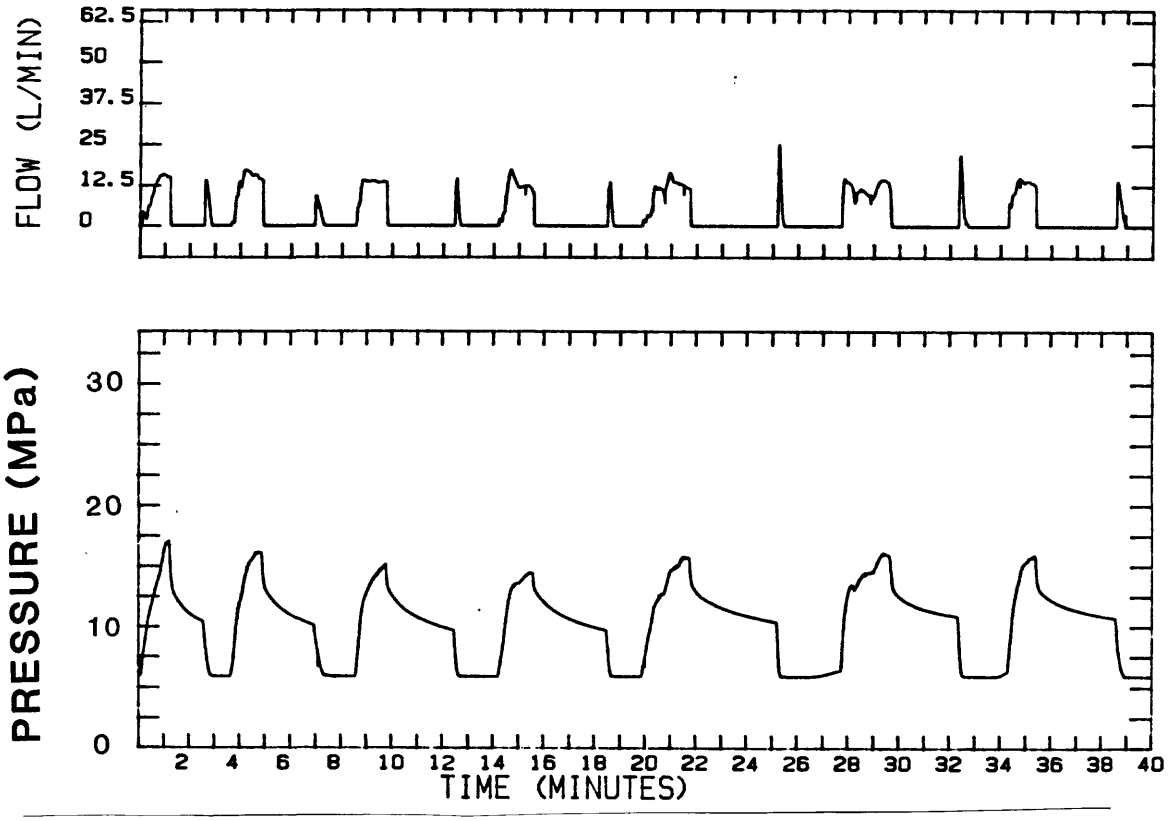

Figure 14. Pressure-time record for the test at 593 m.

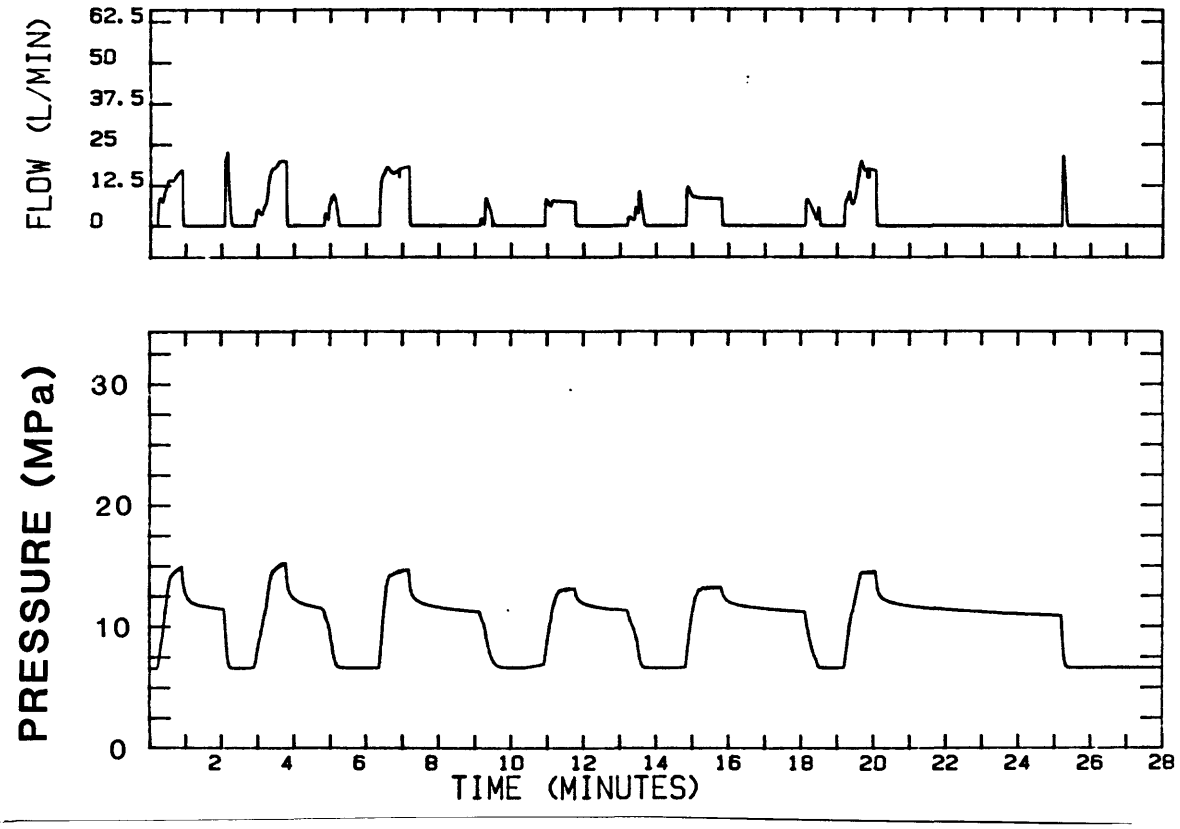

Figure 15. Pressure-time record for the test at 668 m.

Test I was run at 709 m depth in fine sandstone. A pressure-time record for the test is shown in fig. 16. The initial breakdown pressure was 15.1 MPa and Pr was 12.0 to 12.5 MPa. From the inflection point method, the best ISIP value was 17.7 MPa. From the nonlinear regression method it was 15.9 MPa. No impression was taken of the interval. The computed maximum horizontal stress is 28.2 to 32.3 MPa.

Test J was done at 751 m in a silicic sandstone. A pressure-time record for the test is shown in fig. 17. The breakdown pressure was 31.6 MPa. The fracture reopening pressures were too ambiguous to obtain an estimate of SHmax. The best ISIP pick from the inflection point method was 24.8 MPa and the best pick from the nolinear regression method was 22.9 MPa. The impression packer revealed a new fracture striking N8W.

BOREHOLE TELEVIEWER STUDIES

Televiewer Logging

The purpose of the televiewer log was to inspect the borehole conditions, determine the distribution of natural fractures and bedding planes, and characterize any borehole breakouts. The log coverage was from 771 m to the bottom of the casing at 30m. One log was run after tests had been completed at 87m, 152m, 174m, and 218m, but before testing had been done at lower depths.

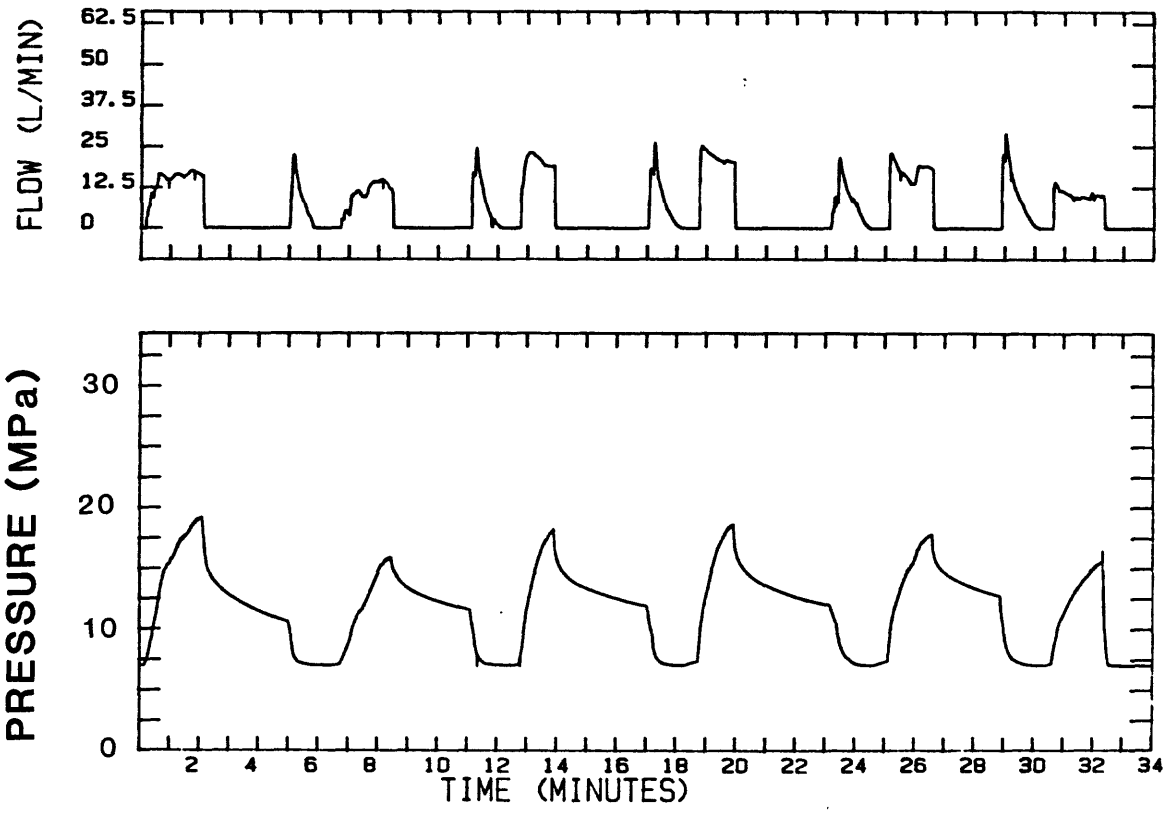

Figure 16. Pressure-time record for the test at 709 m.

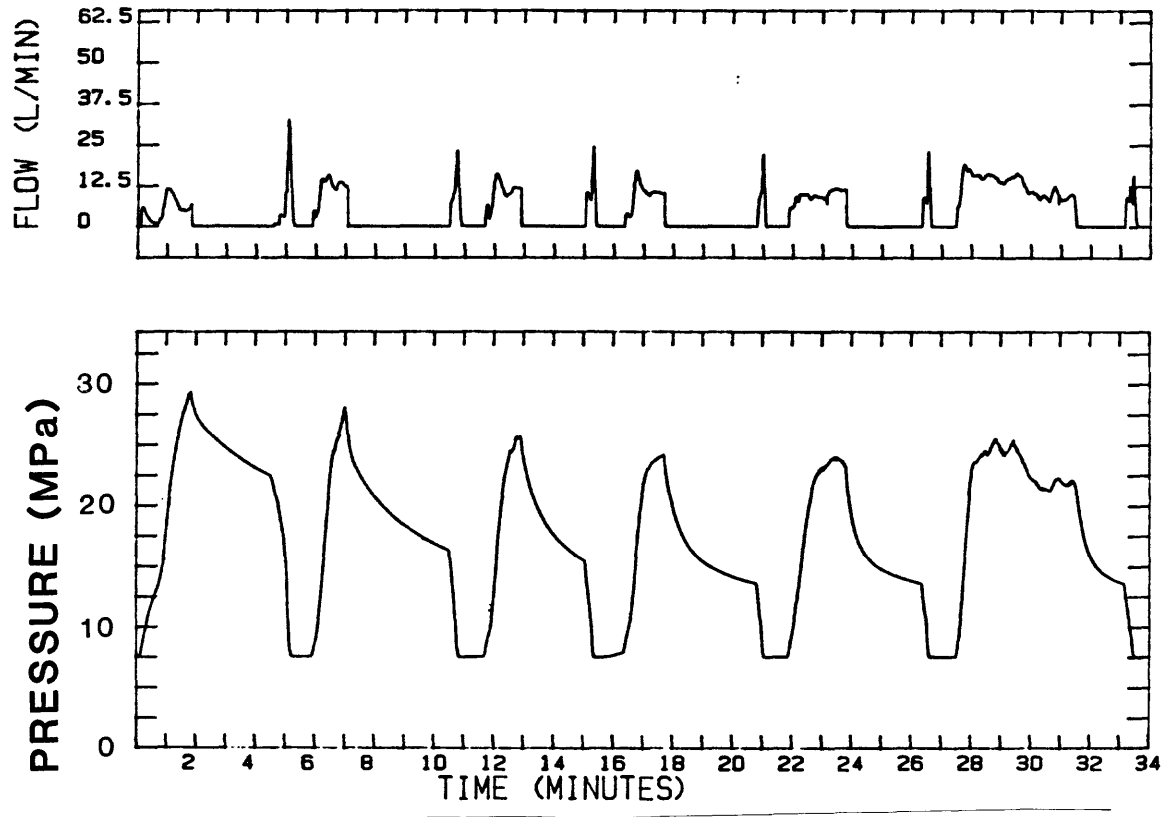

Figure 17. Pressure-time record for the test at 751 m

The borehole televiewer consists of a centralized logging sonde with a rotating peizoelectric transducer that scans the borehole wall with pulses of 1 MHz acoustic energy. The transducer rotates at 3 revolutions per second, emitting and receiving 600 pulses per revolution. A flux-gate magnetometer in the tool triggers each time the transducer sweeps past magnetic north so that the azimuth, amplitude, and two-way travel time of each pulse can be determined. The transducer describes a spiral up the borehole as the log is run at 1.5 m per minute. The signal is transmitted through the logging cable to the surface for processing. The full waveform of the signal was recorded on magnetic tape, along with the compass signal and depth information.

At the surface, the signal is displayed as a function of brightness on the z-axis of a three axis oscilloscope. The field log (fig. 18) consists of a series of polaroid pictures which display an image of the inside of the borehole as if it were split down the middle along magnetic north and laid flat. Dipping planar discontinuities, such as fractures, project as sinusoidal traces on the log. The shape of the sinusoid provides a means of determining the strike and dip of the fracture (see Zemanek, et al., 1970). The complete televiewer log is presented in Appendix B.

Borehole Breakouts

Borehole breakouts are stress-induced enlargements of the borehole that result in a preferred orientation of the long axis of the cross-sectional shape of the hole (Bell and Gough, 1979; Springer et al., 1984; Zoback et al., 1985). The stress concentrations around the borehole, given by solution of the Kirsch equations and shown in fig. 6, cause the maximum tangential stress to be 3SHmax - Shmin along the azimuth of Shmin. When this stress exceeds the compressives strength of the rock, the borehole wall fails, causing the hole to elongate in the direction of Shmin.

Interpretation of borehole breakouts requires analysis of the travel-time of sonic pulses. Digital analysis of the travel-time data is currently underway. The breakouts reported here were first picked from the amplitude record on the field log and were then verified by displaying the travel-time on an oscilloscope. Breakouts sometimes appear on the televiewer log as vertical dark bands 180 degrees apart. This is because the reflected signal amplitude decreases in the failed portion of the borehole. Vertical dark bands, however, can also be caused by an off-centered logging tool. This happens because the incident beam on the borehole wall is oblique and is reflected away from the transducer (Taylor, 1983). This phenomenon is shown schematically in fig. 19.

In order to distinguish breakouts from the off-centered phenomenon, the waveform of the signal is used. By playing the waveform through the z-axis of the scope and playing a single

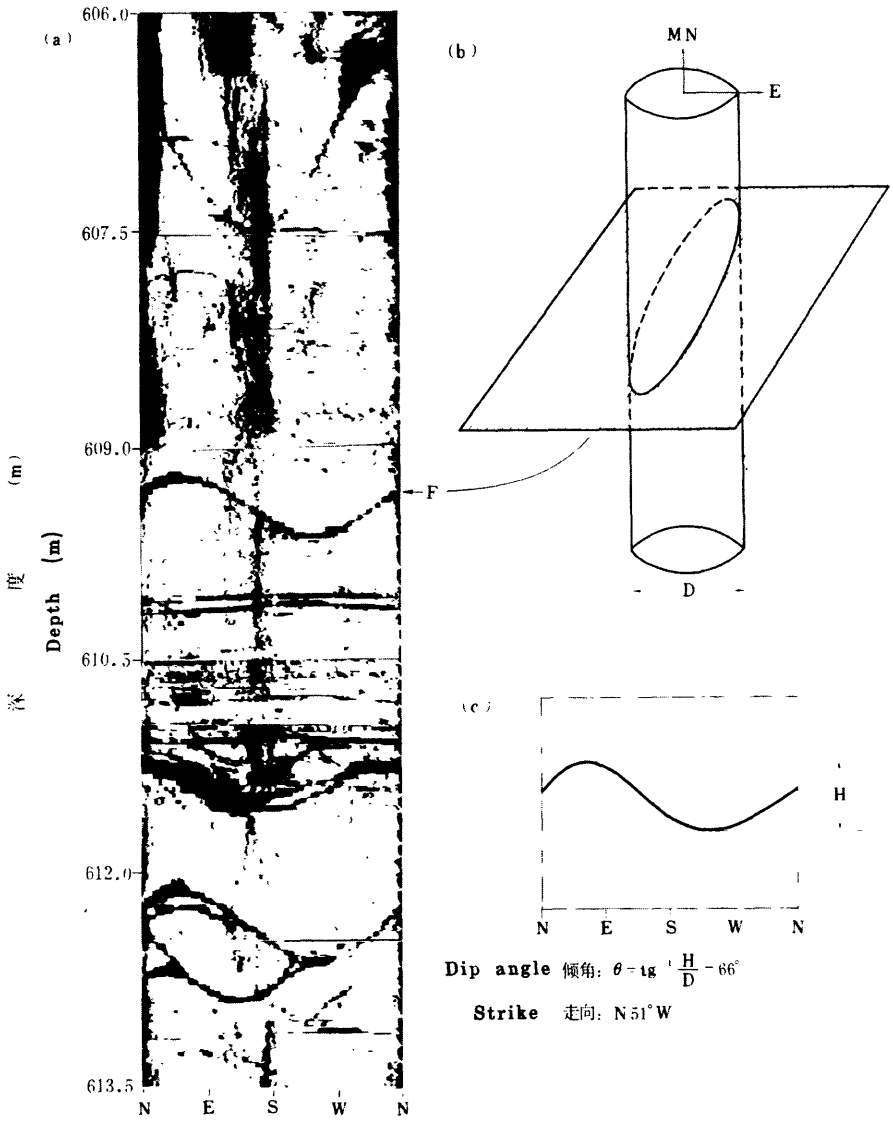

剑川钻孔井下电视测井图象

(a) 实际测井图象, 裂隙F呈现在测井图象上的几何形态

(b) 裂隙F与钻孔相交状态

(c) 裂隙F倾角和走向计算

Televiewer logging image at Jianchuan (Nov. 1986)

(a) The logging image from 606.0 to 613.5 m, Geometry of fracture F on it.

(b) Formation of fracture F crossing the hole.

(c) Calculated dip and strike of fracture F.

Figure 18. Example of a televiewer log showing the strike and dip of an inclined fracture.

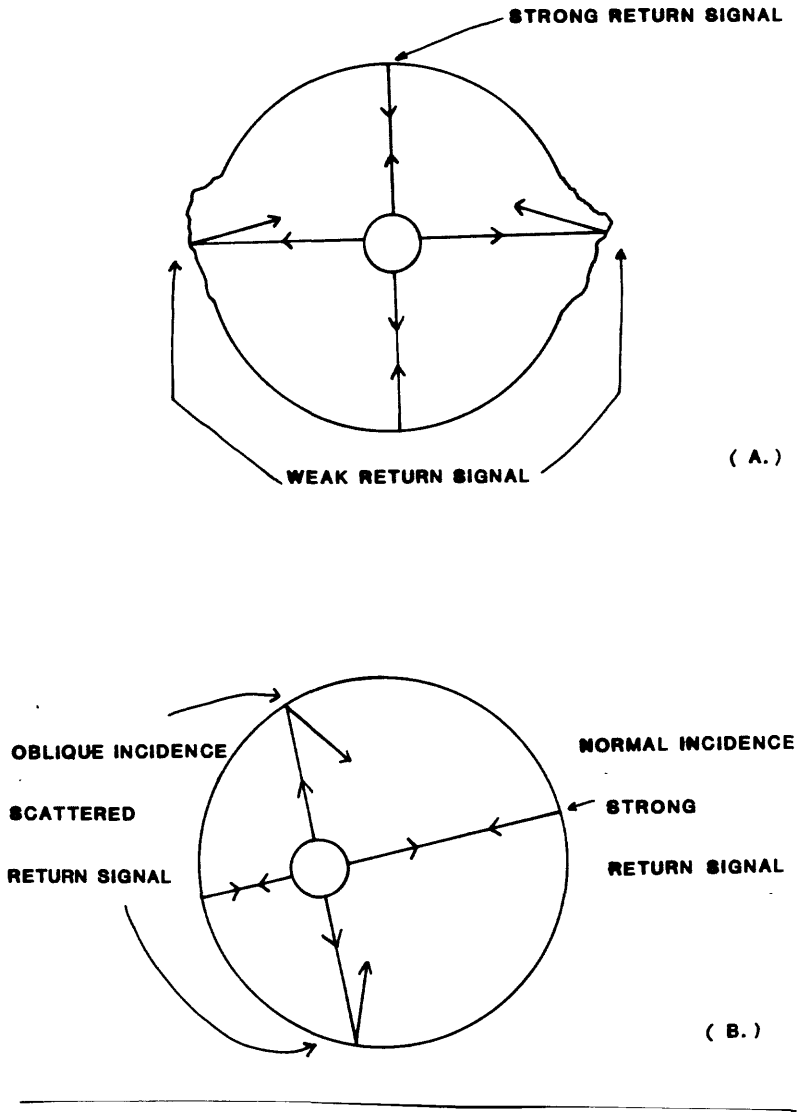

Figure 19. Schematic diagram showing the location of zones of low reflectance on a televiewer image due to an off-centered logging tool and to a borehole breakout.

sweep of the transducer through the y-axis, a plot of travel-time vs azimuth is produced. This plot can then be converted to a cross-section providing the shape of the hole and position of the tool. The calculated cross section from 451.5 m depth is shown in fig. 20.

Twenty-nine breakout zones were identified, representing 44.5 m, or about 6 percent of the length of the borehole. The breakouts have consistent azimuths (fig. 21) averaging about 105 (N75W-S75E). This yields an average maximum stress orientation of N15E. A plot of breakout azimuths vs depth (fig. 22) indicate a large dispersion about the mean between 400 and 600 m. Below that depth, the breakouts are more consistent.

DISCUSSION

The four shallowest tests show that both SHmax and Shmin are higher than Sv, indicating a thrust faulting stress regime (fig. 23). At 174 m and 218 m, the pressure records and televiewer data show evidence that horizontal fractures have been opened, although vertical fractures may have also been created. This is also consistent with a least principal stress that is oriented vertically. The lower tests show the stresses crossing over into the strike-slip regime where SHmax > Sv $\geq$ Shmin.

The likelyhood of renewed movement on favorably oriented fault planes is related to the coefficient of friction, μ , the pore pressure, Po, and the maximum and minimum principal stresses, S1 and S3 (Zoback and Healy, 1984) by the following relationship:

$$(S1 - Po)/(S3 - Po) = [(\mu^2 + 1)^{1/2} + \mu]^2 \qquad [3]$$

Taking the case of thrust faulting and rearranging, the relationship is:

$$SHmax = (Sv - Po)\,[(\mu^2 + 1)^{1/2} + \mu]^2 + Po \qquad [4]$$

A detailed study of friction for a wide variety of rock types (Byerlee, 1978) shows that for most rocks when the normal stress is greater than 5 MPa, the frictional coefficient is between 0.6 and 1. Thus, it can be argued that the likelyhood of movement on favorably oriented trust faults can be assessed by using the relationship in [6] and applying it to the in-situ stress data. The calculated values of SHmax for frictional coefficients of 0.6 and 1 are shown in fig. 23. The envelope defined by the curves represents the values for SHmax for which movement on favorably oriented thrust faults might be expected. Because Byerlee's (1978) relationship does not apply under low normal stresses, the envelope is drawn only for depths greater than 200 m. Similar calculations, using the maximum horizontal shear stress show that the lower tests do not fall within the failure envelope for strike-slip faulting.

From this data we cannot say anything about the stability of

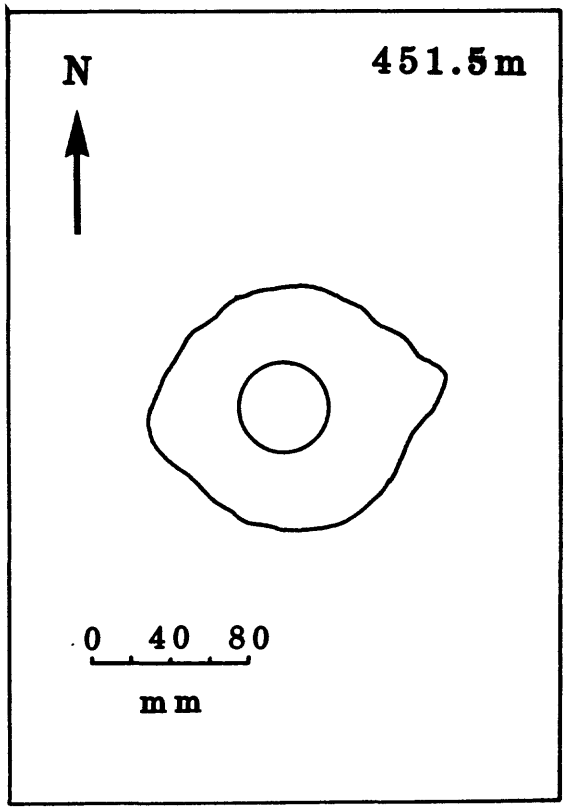

Figure 20. Cross-sectional shape of the hole at 451.5 m showing a well developed breakout.

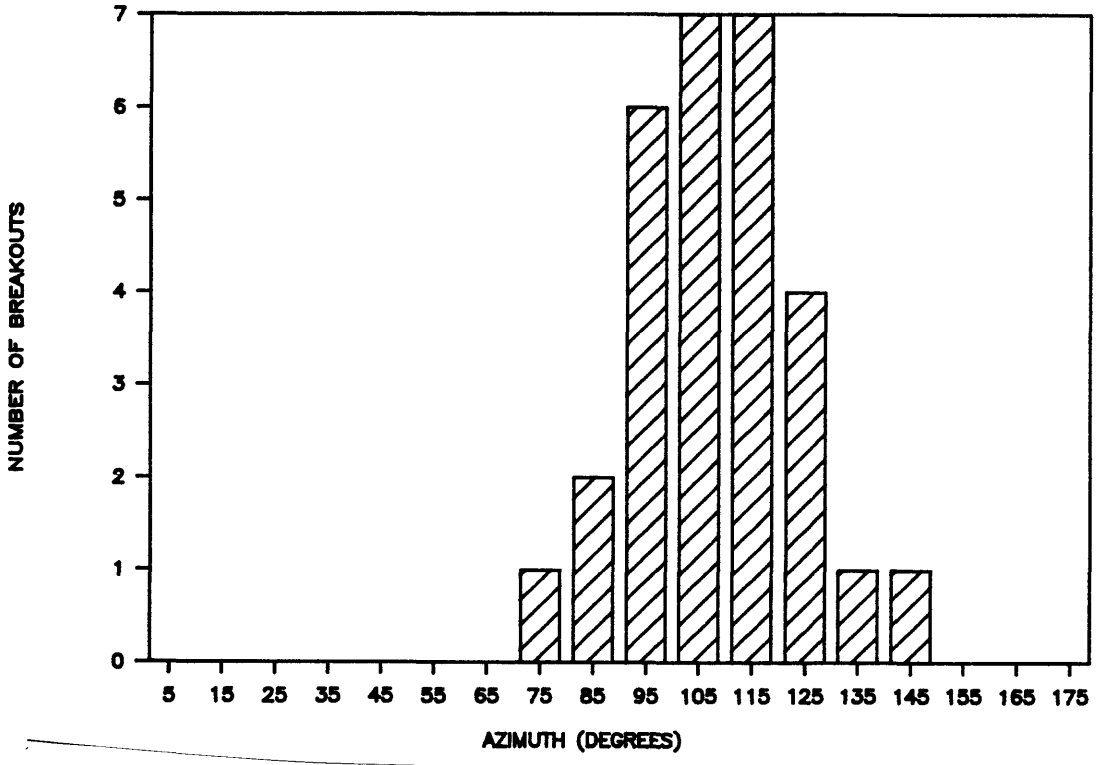

Figure 21. Histogram showing the orientations of breakouts.

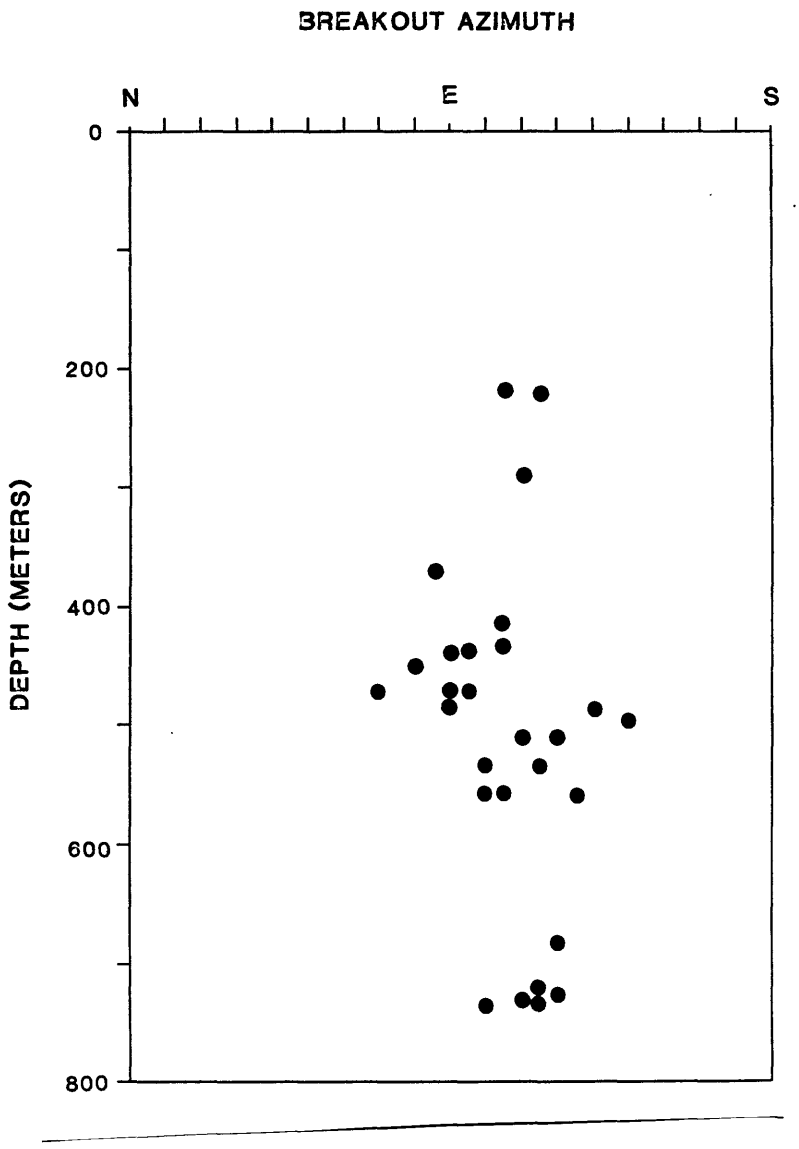

Figure 22. Plot of breakout azimuth vs depth.

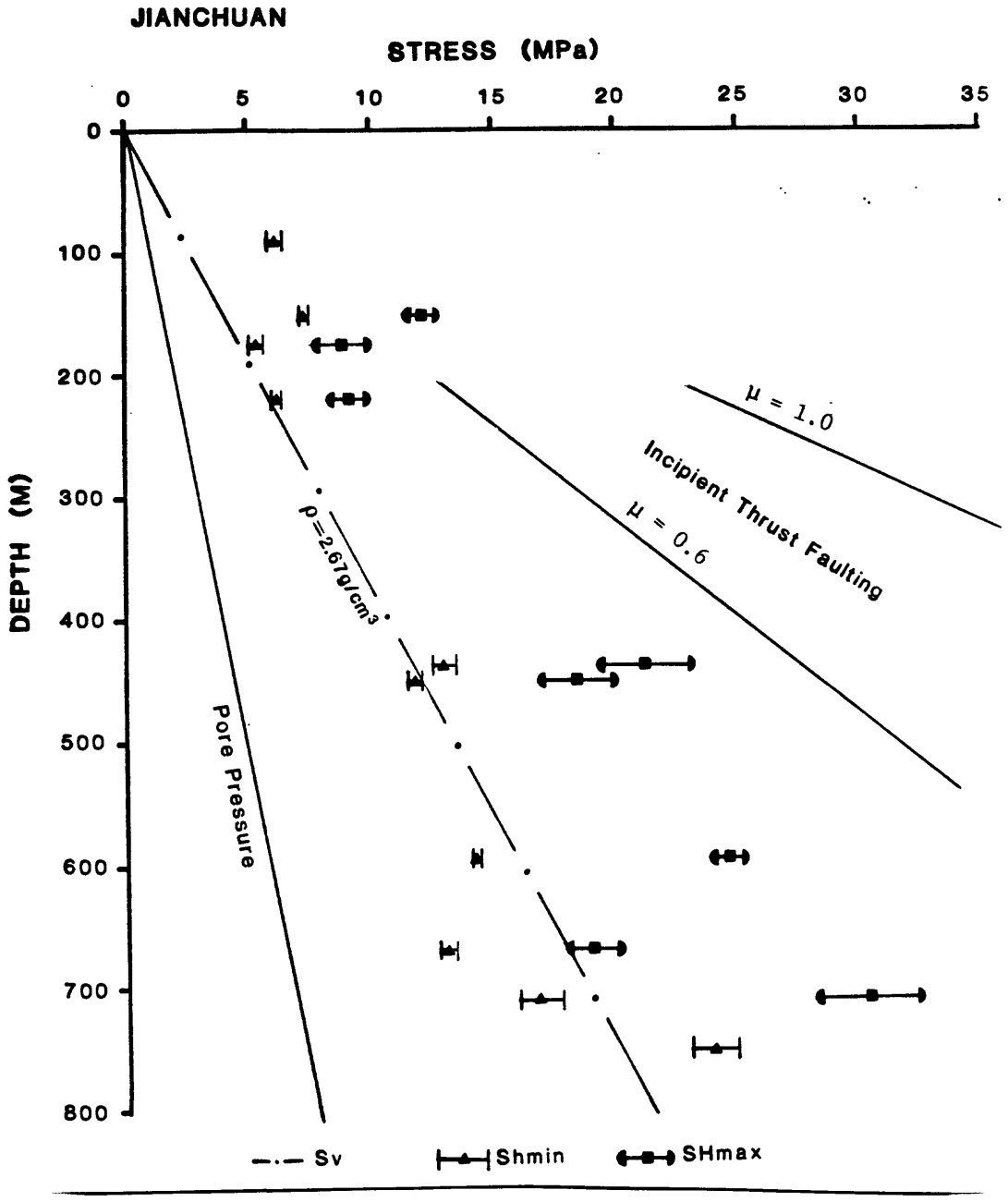

Figure 23. Plot of SHmax, Shmin, Sv, and Po vs depth in the Jianchuan hole. The envelope for frictional failure on favorably oriented thrust faults is shown for frictional coefficients between 0.6 and 1.0.

faults at seismogenic depths. Detailed mapping and studies of fault plane solutions (Kan et al., 1977; Allen et al., 1984) show that normal and strike-slip faulting are active in this region. Shallow thrust faulting stress regimes that change to strike-slip faulting at greater depth have been reported elswhere (Zoback et al., 1980; Brace and Kohlstedt, 1980) and are not unusual.

The high relief in the vicinity of the Jianchuan site, may effect the shallow stress field. Gravitational loading may add to the horizontal stress component perpendicular to the axis of the valley. The shallowest test indicates a hydrofracture orientation perpendicular to the valley axis. At depth, the SHmax direction, derived from breakouts becomes about N15E. A tentative conclusion from this data is that topographic loading is influencing the near-surface stresses and that the topographic affect diminishes with depth. Because of this possible topographic affect on the near-surface stresses, it would be advantageous to measure in-situ stresses at greater depths in order to better understand the tectonic regime.

CONCLUSIONS

The main conclusions drawn from the hole are:

1. In the upper 200 m, both horizontal stresses are greater than the calculated vertical stress indicating a thrust faulting stress regime. Below 200 m, the stresses approach transition to a strike-slip stress regime.

2. At shallow depths, hydraulic fracture orientations and borehole breakouts show some variation in orientation, suggesting a local phenomenon, such as gravitational loading from the topography, may be influencing the stress directions.

ACKNOWLEDGEMENTS

We thank Dave Russ and Jack Healy for their support of the project. Zhang Juin kept the electronic equipment running and helped run the televiewer log. Liu Yujuo logged the core and helped interpret the televiewer pictures.

REFERENCES

Allen, C.R., Gillespie, A.R., Han Yuan, Sieh, K.E., Zhang Buchun, and Zhu Chengnan, 1984, Red River and associated faults, Yunnan Province, China: Quaternary geology, slip rates, and seismic hazard: Geological Society of America Bulletin, v.95, pp.686-700.

Bell, J.S. and Gough. D.I., 1979, Northeast-southwest compressive stress in Alberta; evidence from oil wells: Earth and Planetary Science Letters, v.45, pp.475-482.

Brace, W.F. and Kohlstedt, D.L., 1980, Limits on lithospheric stress imposed by laboratory experiments: Journal of Geophysical Research, v.85, pp.6248-6252.

Bredehoeft, J.D., Wolff, R.G., Keys, W.S., and Shuter, E., 1976,

Hydraulic fracturing to determine the regional in-situ stress field, Piceance Basin, Colorado: Geological Society of America Bulletin, v.87, pp.250-258.
Byerlee, J.D., 1978, Friction of rock: Pure and Applied Geophysics, v.116, pp.615-626.
Geologic Bureau of Yunnan Province, 1975, Geologic map of the Lan Ping area: Scale = 1:200,000.
Gronseth, J.M. and P.R. Kry, 1983, Instantaneous shut-in pressure and its relationship to the minimum in-situ stress: in, Zoback, M.D. and B.C. Haimson, convenors,Hydraulic Fracturing Stress Measurements, National Academy Press, pp.55-60.
Haimson, B.C. and Fairhurst, C., 1967, Initiation and extension of hydraulic fractures in rock: Society of Petroleum Engineers Journal, v.7, pp.310-318.
Haimson, B.C. and M.Y. Lee, 1987, The state of stress and natural fractures in a jointed preCambrian rhyolite in south-central Wisconsin: Proceedings of the 28th U.S. Symposium on Rock Mechanics, A.A. Balkema, Rotterdam, Boston, pp.231-240.
Hickman, S.H. and Zoback, M.D., 1983, The interpretation of hydraulic fracturing pressure-time data for in-situ stress determination: Hydraulic Fracturing Stress Measurements, Proceedings of a Workshop, December 2-5, 1981, pp.44-54.
Hubbert, M.K. and Willis, D.G., 1957, Mechanics of hydraulic fracturing: Journal of Petroleum Technology, v.9, pp.153-168.
Jaeger, J.C. and N.G.W. Cook, 1976, Fundamentals of rock mechanics: (2nd edition), Chapman Hall, John Wiley and Sons, New York.
Kan Rongju, Zhang Sichang, Yan Fengtong, and Yu Linsheng, 1977, Present tectonic stress field and its relation to the characteristics of recent tectonic activity in southwest China (in Chinese): Acta Geophysica Sinica, v.20, pp.96-109.
McGarr, A. and Gay, N.C., 1978, State of stress in the earth's crust: Annual Reviews of Earth and Planetary Science, v.6, pp.405-436.
Muskat, M., 1937, The use of build-up of bottom-hole pressures: Transactions, American Institute of Mining and Metallurgical Engineers, v.123, pp.44-48.
Springer, J.E., Zhai Qingshan, and J.F. Svitek, 1987, Summary of the geologic setting and televiewer logs from the Yongping test well, Yunnan Province, China: U.S. Geological Survey, Open-file report, 87-427, 28p.
Springer, J.E., Thorpe, R.K., and McKague, H.L., 1984, Borehole elongation as an indicator of tectonic stress orientation at the Nevada Test Site: Geological Society of America, Abstracts with Programs, v.16, no.5, p.334.
Taylor, T.J., 1983, Interpretation and application of borehole televiewer surveys: Society of Professional Well Log Analysts, 24th Annual Logging Symposium, paper no. QQ, 19p.
Zemanek, J., Glenn, E.E., Norton, L.J., and Caldwell, R.L., 1970, Formation evaluation by inspection with the borehole televiewer: Geophysics, v.35, no.2, pp.245-269.
Zoback, M.D. and Healy, J.H., 1984, Friction, faulting, and in-situ stress: Annales Geophysicae, v.2, no.6, pp.689-698.

Zoback, M.D., Moos, D., Mastin, L.G., and Anderson, R.N., 1985, Well bore breakouts and in-situ stress: Journal of Geophysical Research, v.90, no. B7, pp.5523-5530.
Zoback, M.D., Tsukahara, H., and Hickman, S.H., 1980, Stress measurements at depth in the vicinity of the San Andreas fault; implications for the magnitude of shear stress at depth: Journal of Geophysical Research, v.85, pp.6157-6173.
Zoback, M.L. and Zoback M.D., 1980, State of stress in the conterminous United States: Journal of Geophysical Research, v.85, pp.6113-6156.

APPENDIX A

Cycle by Cycle Results of the Hydrofracturing Tests

TABLE 1A
ISIP Determinations
(Downhole Pressures in MPa)

Cycle	Method IP	LF	NLR	FR
Test A: Depth = 88 m, Po = 0.9 MPa				
1	6.7	--	6.2	--
2	6.4	--	5.7	--
3	6.0	--	5.4	--
4	6.0	6.5	--	--
5	--	--	--	5.8
Best Picks:	6.0	6.5	5.7	5.8
Test B: Depth = 152 m, Po = 1.5 MPa				
1	7.7	--	6.4	--
2	7.7	--	6.2	--
3	7.3	--	6.0	--
4	7.3	7.5	--	--
5	6.7	--	--	--
6	6.3	--	--	--
7	5.3	--	--	--
Best Picks:	7.3	7.5	6.2(ave)	--
Test C: Depth = 174 m, Po = 1.7 MPa				
1	6.9	--	--	--
2	6.5	--	6.1	--
3	5.1	5.7	--	--
4	5.1	--	--	--
5	5.0	--	--	--
6	5.5	--	--	--
7	5.5	--	--	--
8	4.9	--	--	--
Best Picks:	5.1	5.7	6.1	--
Test D: Depth = 218 m, Po = 2.1 MPa				
1	7.6	--	7.7	--
2	6.6	--	6.4	--
3	6.3	--	5.6	--
4	5.6	6.0	--	--
5	5.6	--	--	--
Best Picks:	6.3	6.0	6.4	--

Methods: IP=inflection point, LF=low flow-rate pumping pressure, FR=flow-rate vs pumping pressure, NLR=nonlinear regression.

TABLE 1A (continued)
ISIP Determinations
(Downhole pressures in MPa)

Cycle	Method IP	LF	NLR	FR
Test E: Depth = 437 m, Po = 4.3 MPa				
1	--	--	17.3	--
2	--	--	13.3	--
3	12.5	13.4	12.4	--
4	12.5	--	--	--
5	13.2	--	--	--
6	12.9	--	--	--
Best Picks:	12.5	13.4	12.4	12.7
Test F: Depth = 451 m, Po = 4.4 MPa				
1	13.7	--	--	--
2	11.3	--	--	--
3	12.0	--	--	--
4	11.3	11.5	--	--
5	12.1	--	--	--
6	13.0	--	--	--
Best Picks:	12.0	11.5	--	--
Test G: Depth = 593 m, Po = 5.8 MPa				
1	14.5	--	14.7	--
2	14.5	--	14.3	--
3	14.3	--	13.8	--
4	14.2	--	14.0	--
5	14.5	--	13.8	--
6	14.2	--	14.0	--
7	14.3	--	14.0	--
Best Picks:	14.2	--	14.3	--
Test H: Depth = 668 m, Po = 6.6				
1	13.3	--	17.3	--
2	13.2	--	12.3	--
3	13.3	--	12.7	--
4	13.0	--	12.6	--
5	12.9	--	12.2	--
6	13.0	13.2	12.2	--
7	13.2	--	12.5	--
Best Picks:	13.3	13.2	12.7	--

TABLE 1A (continued)
ISIP Determinations
(Downhole pressures in MPa)

Cycle	Method			
	IP	LF	NLR	FR
Test I: Depth = 709 m, Po = 7.0 MPa				
1	17.0	--	15.9	--
2	16.0	--	15.0	--
3	13.4	--	--	--
4	17.7	--	--	--
5	17.2	--	16.3	--
Best Picks:	17.7	--	15.9	--
Test J: Depth = 751 m, Po = 7.4 MPa				
1	--	--	30.1	--
2	26.5	--	24.9	--
3	24.8	--	22.9	--
4	23.0	--	--	--
5	21.3	--	22.8	--
6	19.5	--	--	--
7	22.5	--	23.5	--
Best Picks:	24.8	--	22.9	--

TABLE 2A
Breakdown and Fracture Reopening Pressures
(Downhole Pressures in MPa)

Test	Cycle	Pb	Pr
A	1	9.4	--
88 m	2	--	8.8
	3		6.7
	4		6.7
Picks		9.4	6.7 to 8.8
B	1	--	--
152 m	2		8.7
	3		8.4
	5		8.0
	6		8.0
	7		7.7
Picks:		no breakdown	8.4 to 8.7
C	1	7.1	--
174 m	2		5.8
	3		5.5
	4		4.8
	5		4.8
	6		4.8
	7		5.1
	8		4.1
Picks:		7.1	5.5 to 5.8
D	1	8.3	--
218 m	2		7.5
	3		7.3
	4		5.6
	5		6.3
Picks:		8.3	7.3 to 7.5
E	1	17.5	--
437 m	3		13.0
	5		15.3
	6		13.5
Picks:		17.5	13.0 to 13.5
F	1	--	--
451 m	3		11.6?
	4		9.5?
	5		13.0?
	6		13.0?
Picks:		no breakdown	11.6 to 13.0?

TABLE 2A (continued)
Breakdown and Fracture Reopening Pressures
(Downhole pressures in MPa)

Test	Cycle	Pb	Pr
G	1	18.3	--
593 m	2		12.4
	3		11.9
	4		12.8
	5		12.3
	6		11.6
	7		12.3
Picks:		18.3	11.9 to 12.8
H	1	15.6	--
668 m	2		13.5
	3		13.7
	4		13.2
	5		12.1
	6		12.3
Picks:		15.6	13.2 to 13.5
I	1	15.1	--
709 m	2		12.0
	3		12.4
	4		12.5
	5		12.0
	6		11.3
Picks:		15.1	12.0 to 12.5
J	1	31.6	--
Picks:		31.6	--

APPENDIX B

Borehole Televiewer Logs

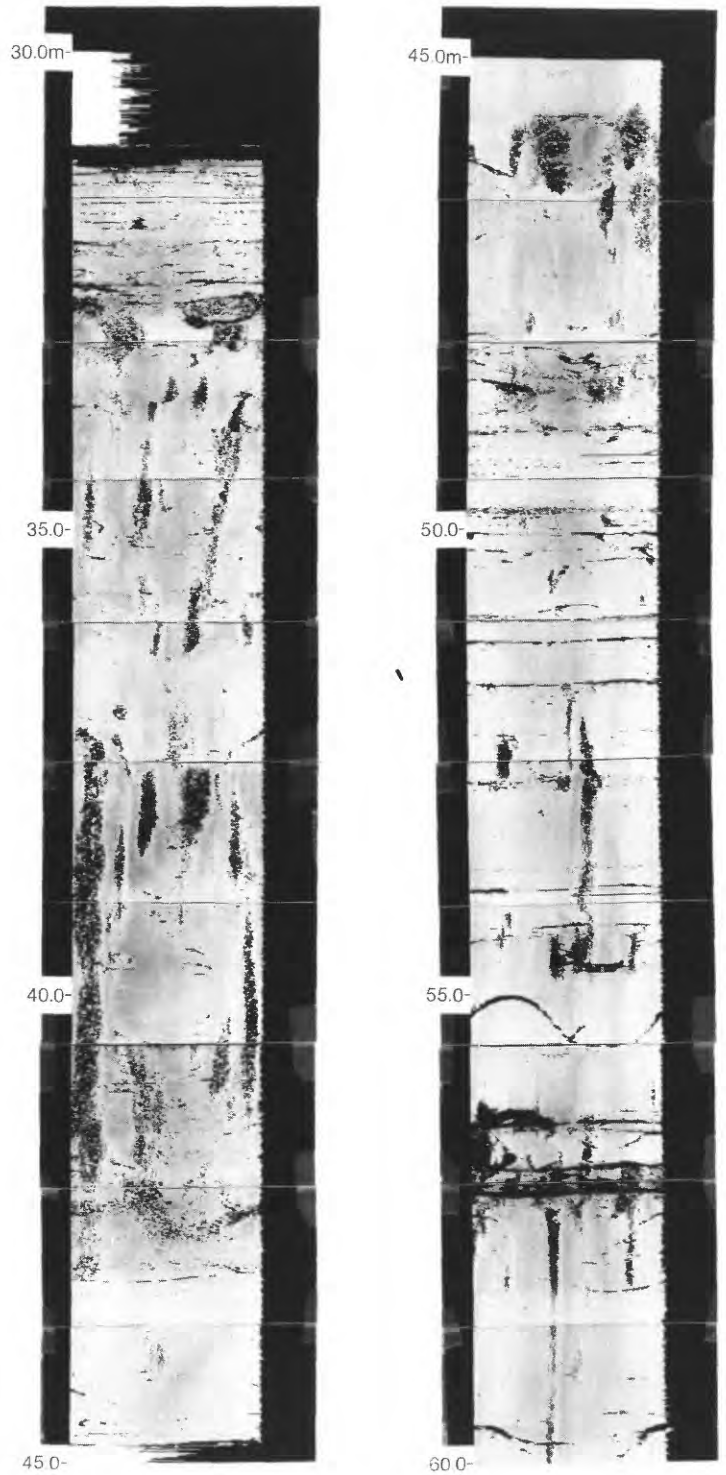
30.0m-
35.0-
40.0-
45.0-
45.0m-
50.0-
55.0-
60.0-

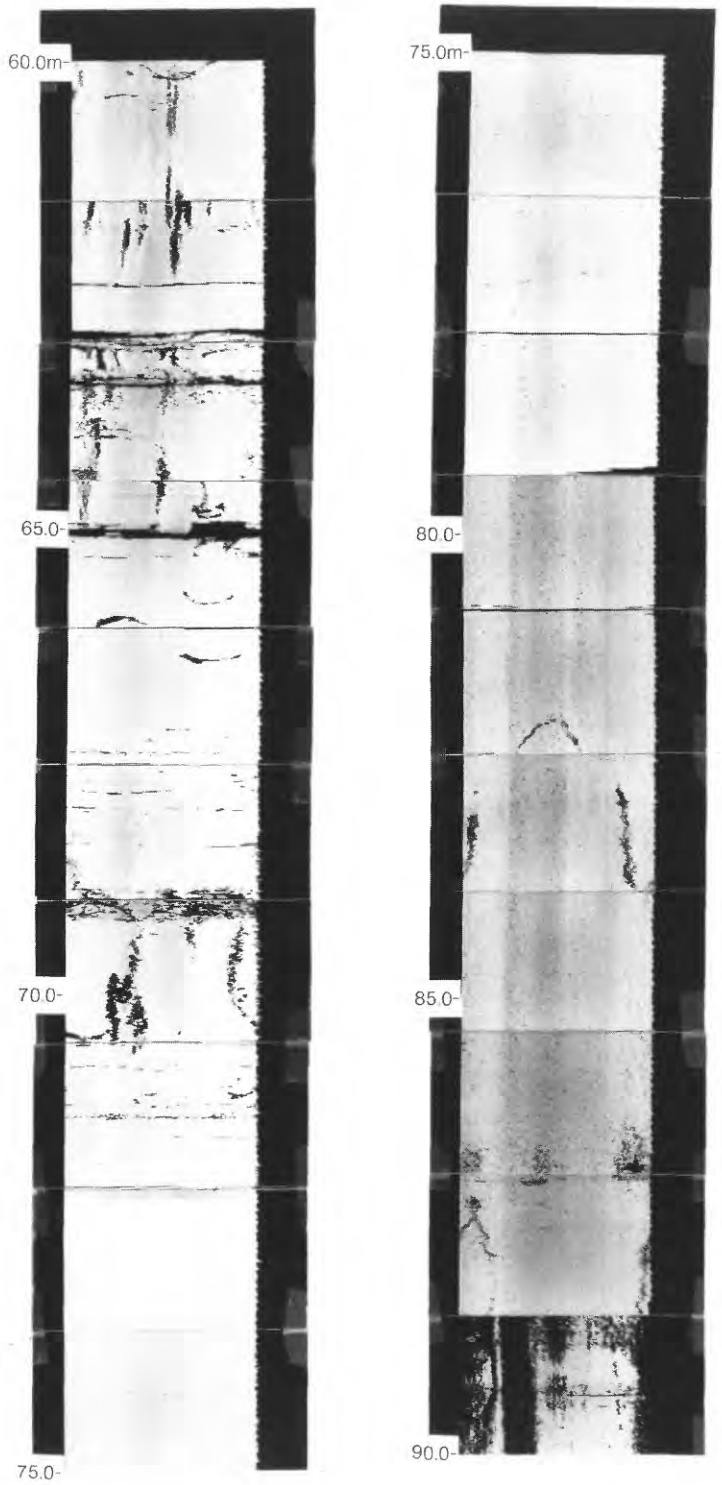
60.0m-
65.0-
70.0-
75.0-
75.0m-
80.0-
85.0-
90.0-

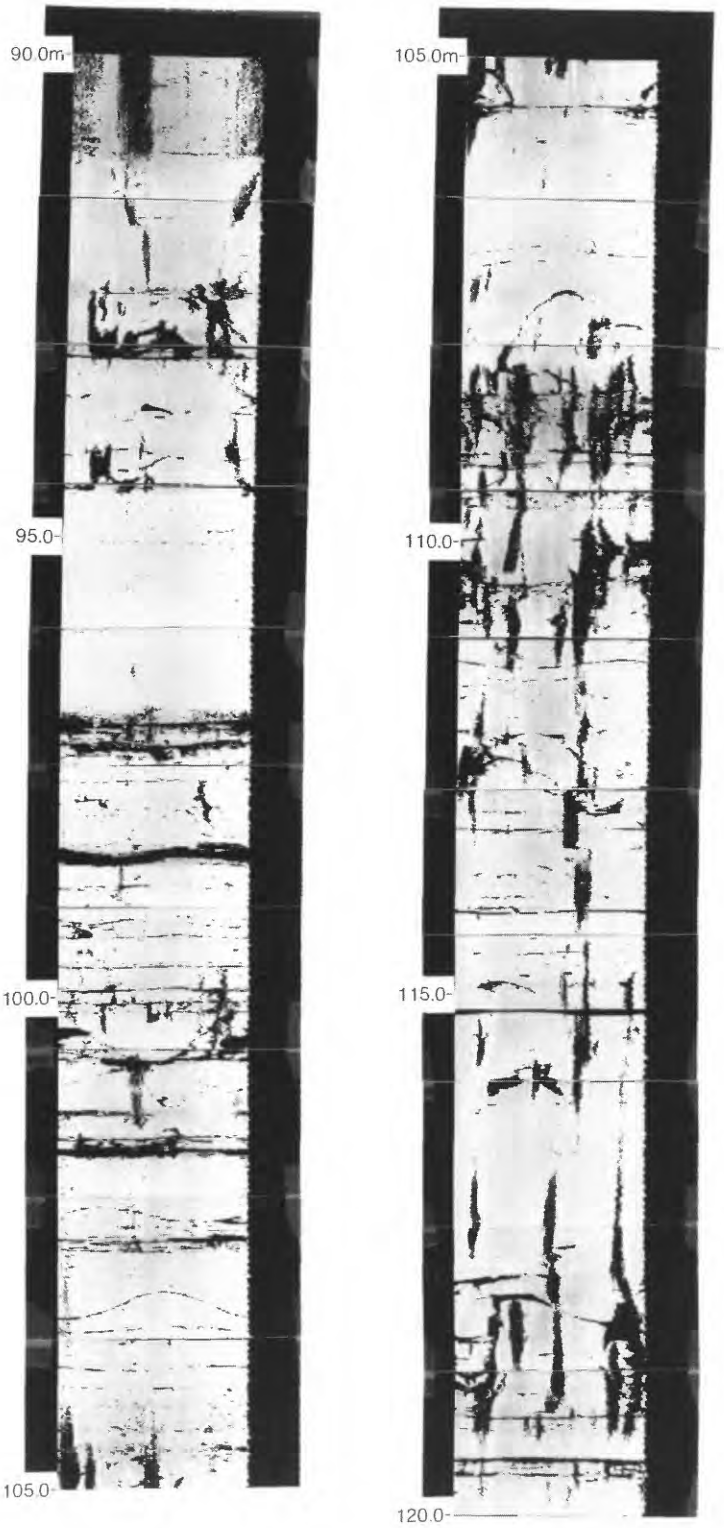
90.0m
95.0
100.0
105.0
105.0m
110.0
115.0
120.0

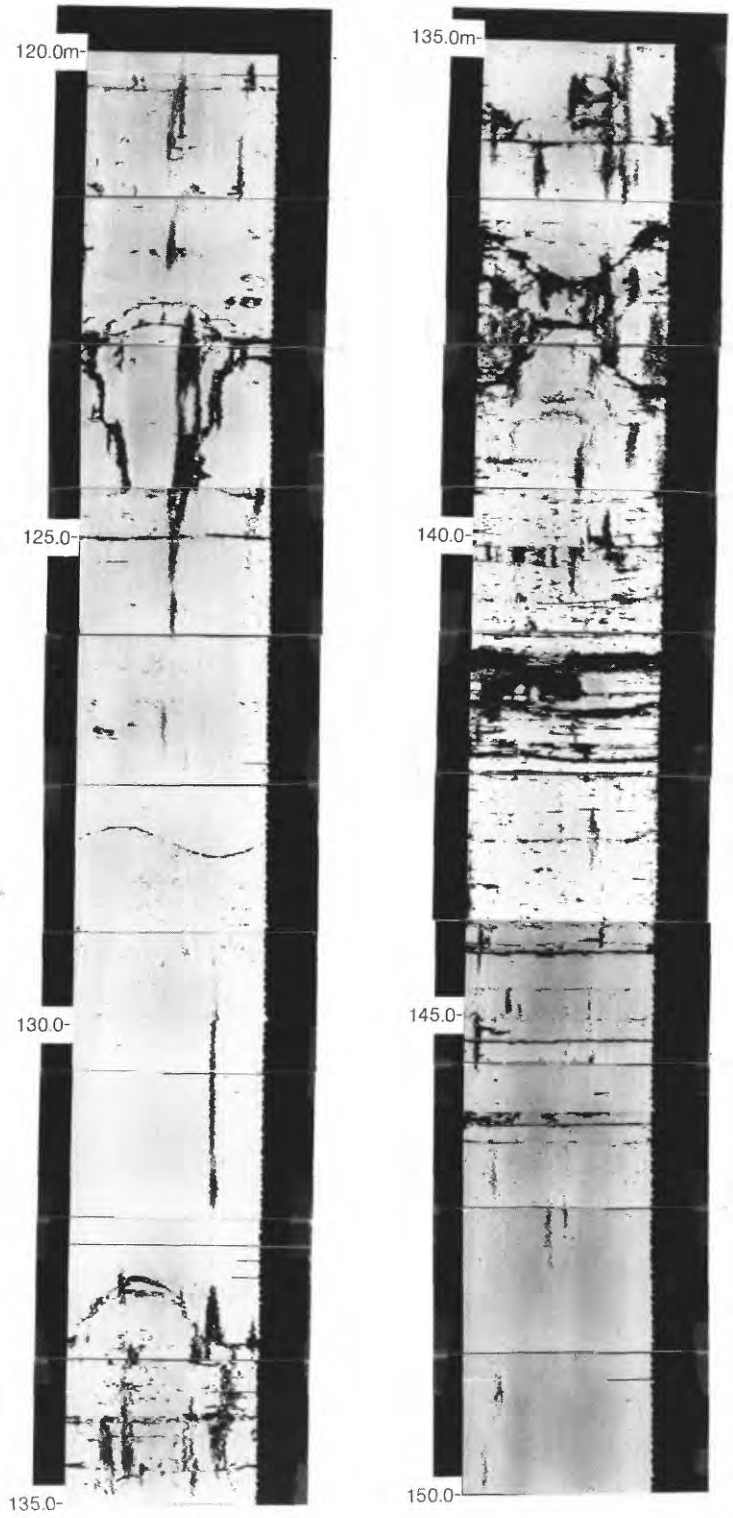
120.0m-
125.0-
130.0-
135.0-
135.0m-
140.0-
145.0-
150.0-

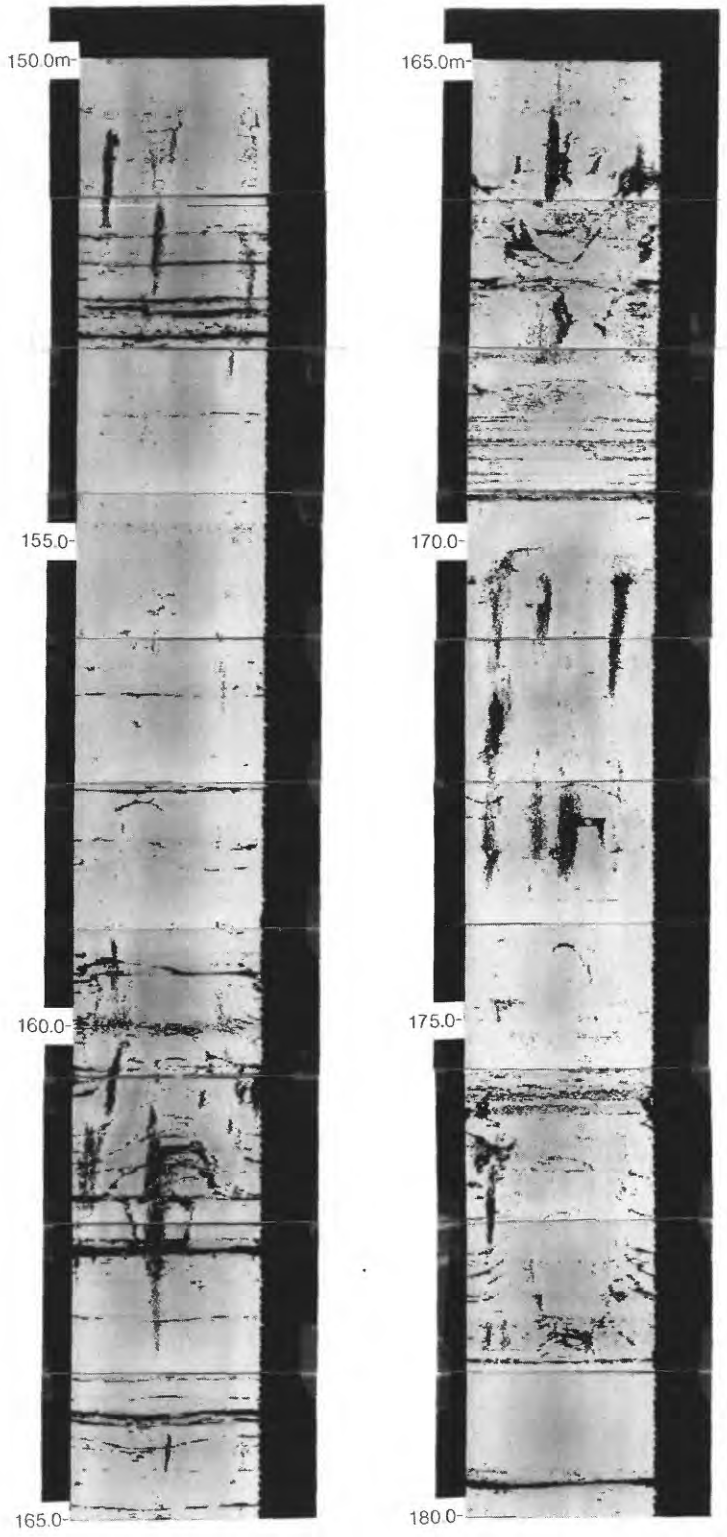
150.0m
155.0
160.0
165.0
165.0m
170.0
175.0
180.0

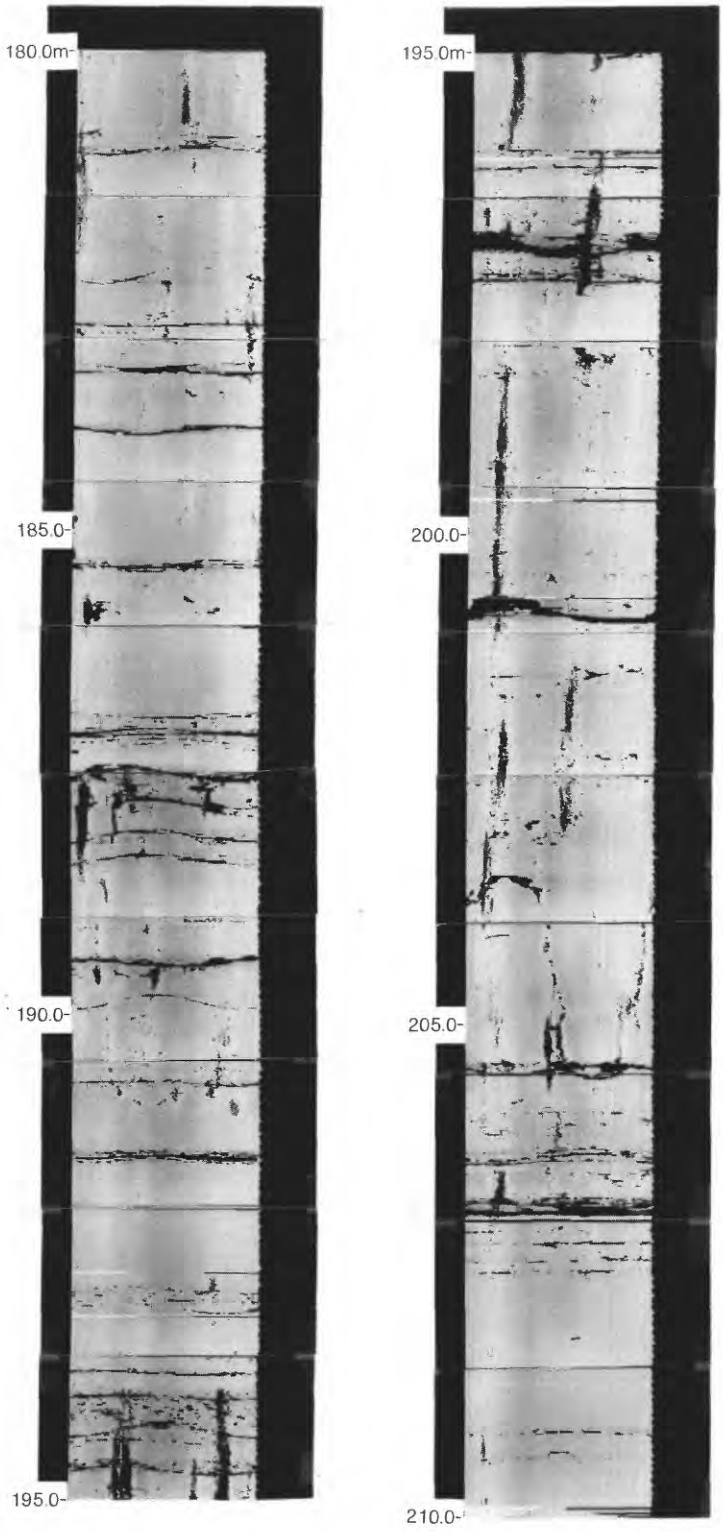
180.0m
185.0
190.0
195.0
195.0m
200.0
205.0
210.0

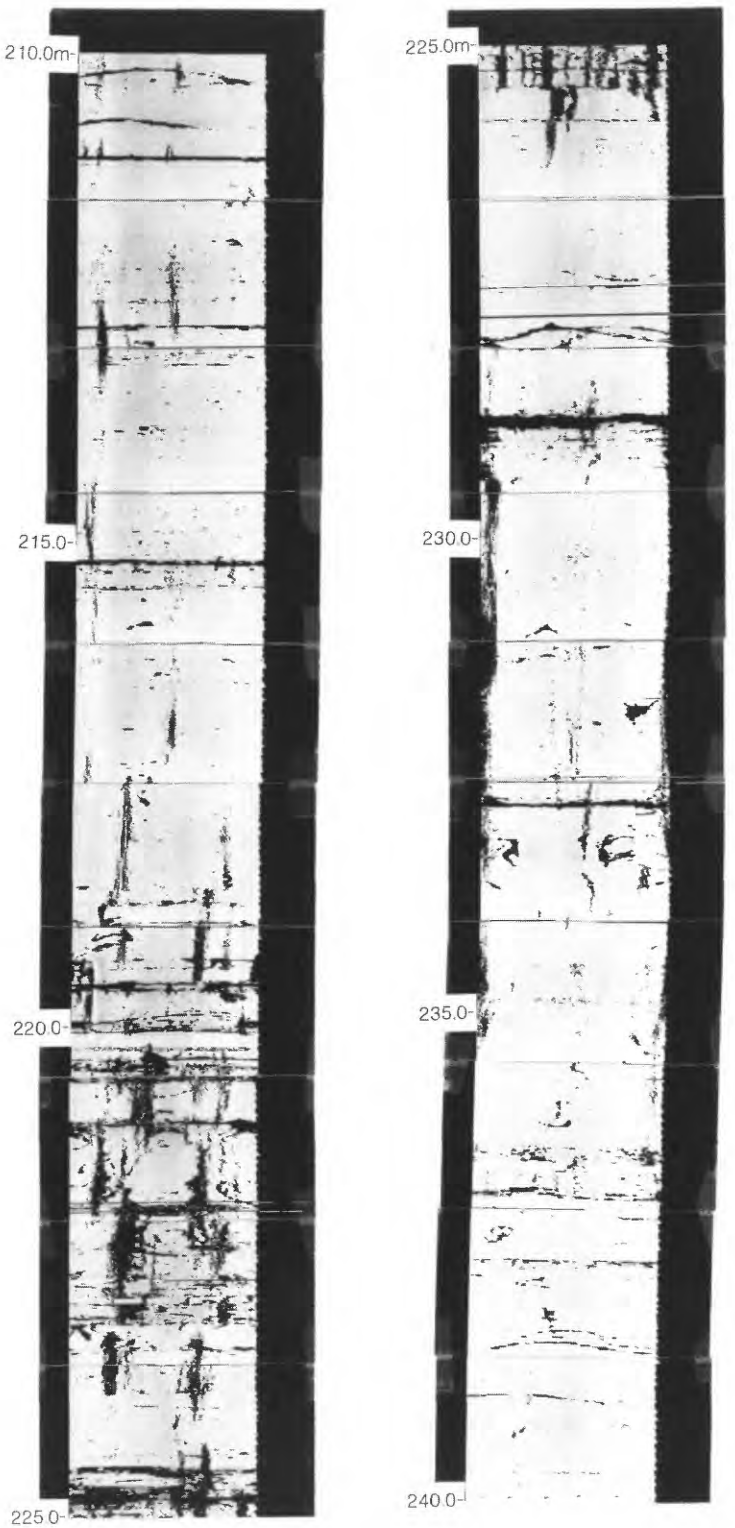
210.0m
215.0
220.0
225.0
225.0m
230.0
235.0
240.0

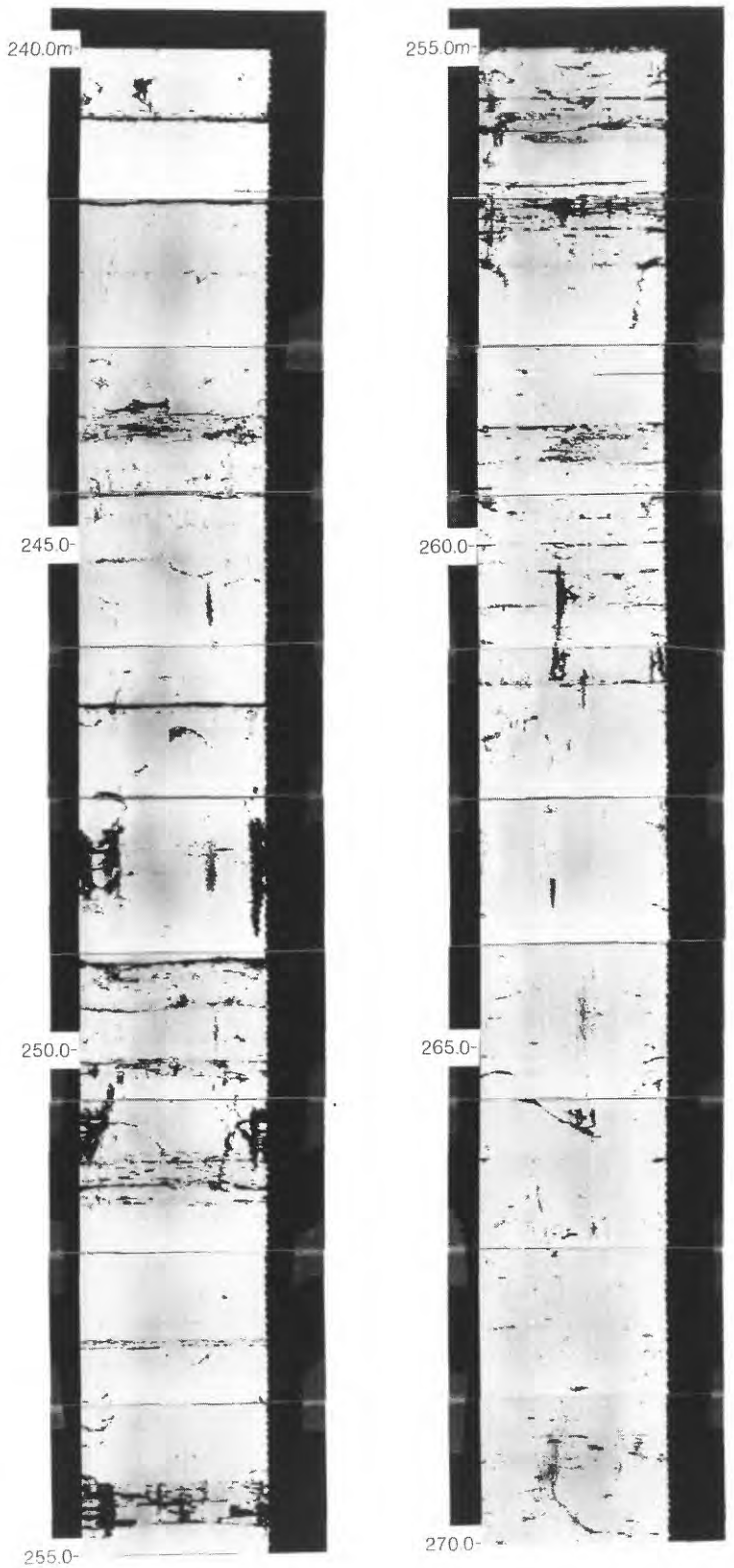
240.0m
245.0-
250.0-
255.0-
255.0m
260.0-
265.0-
270.0-

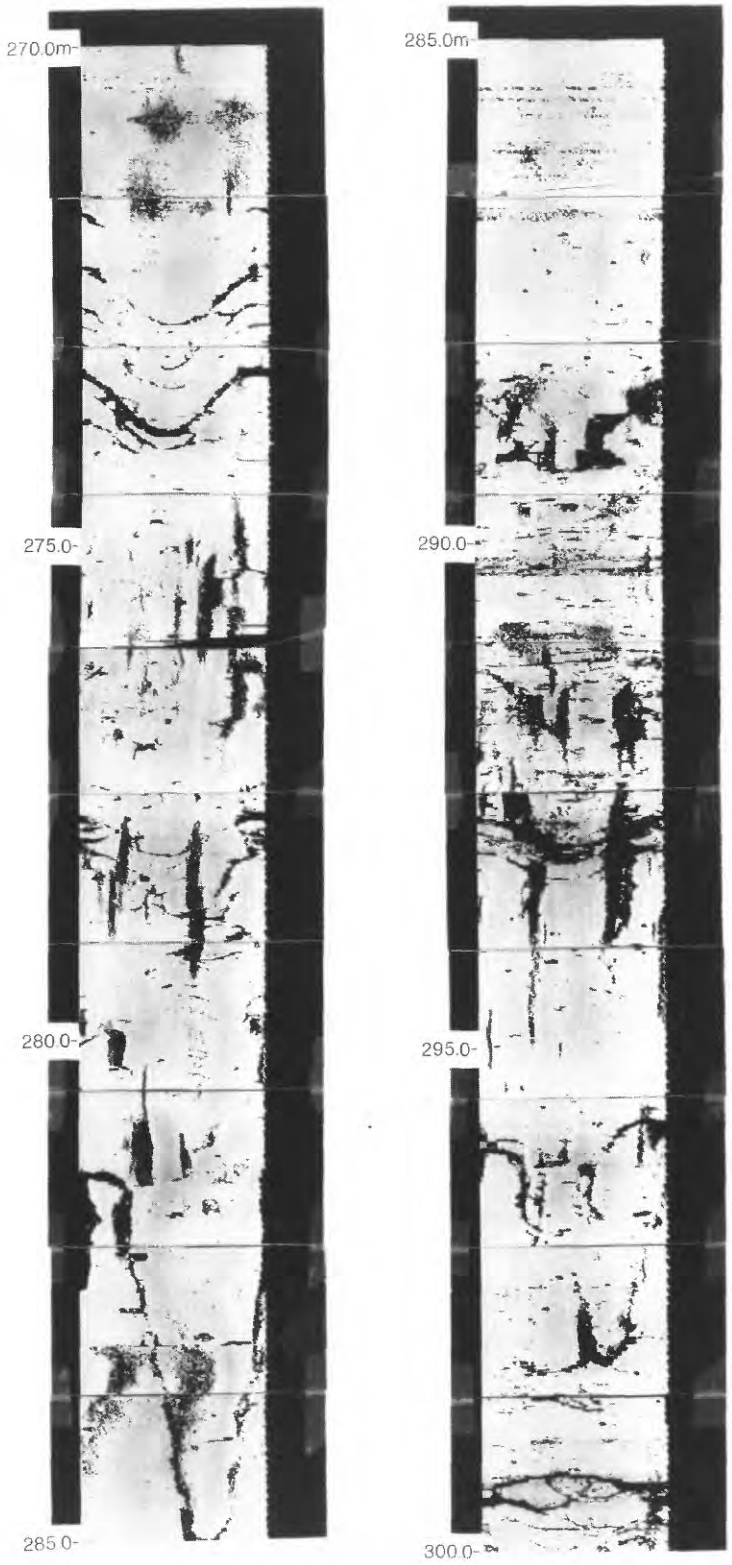
270.0m
275.0
280.0
285.0
285.0m
290.0
295.0
300.0

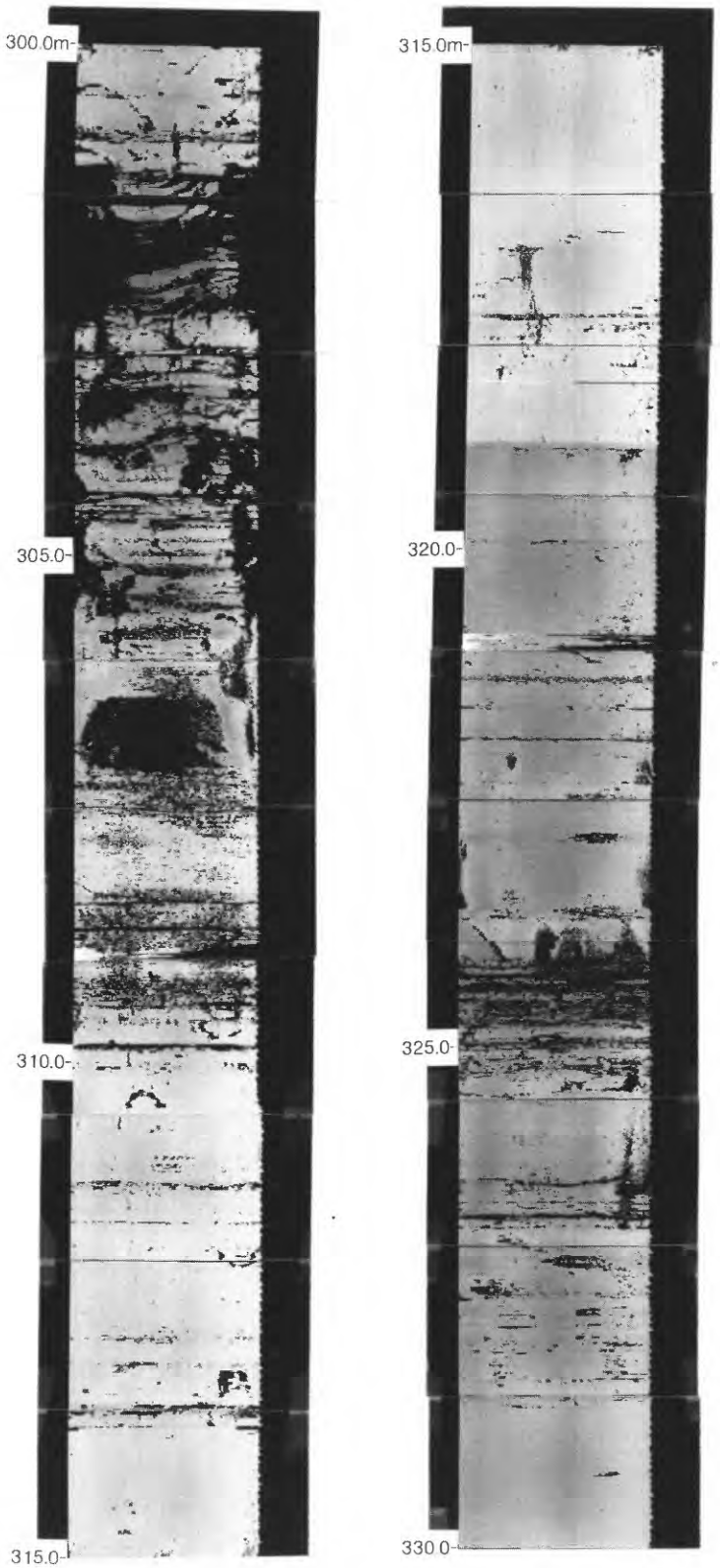
300.0m
305.0
310.0
315.0
315.0m
320.0
325.0
330.0

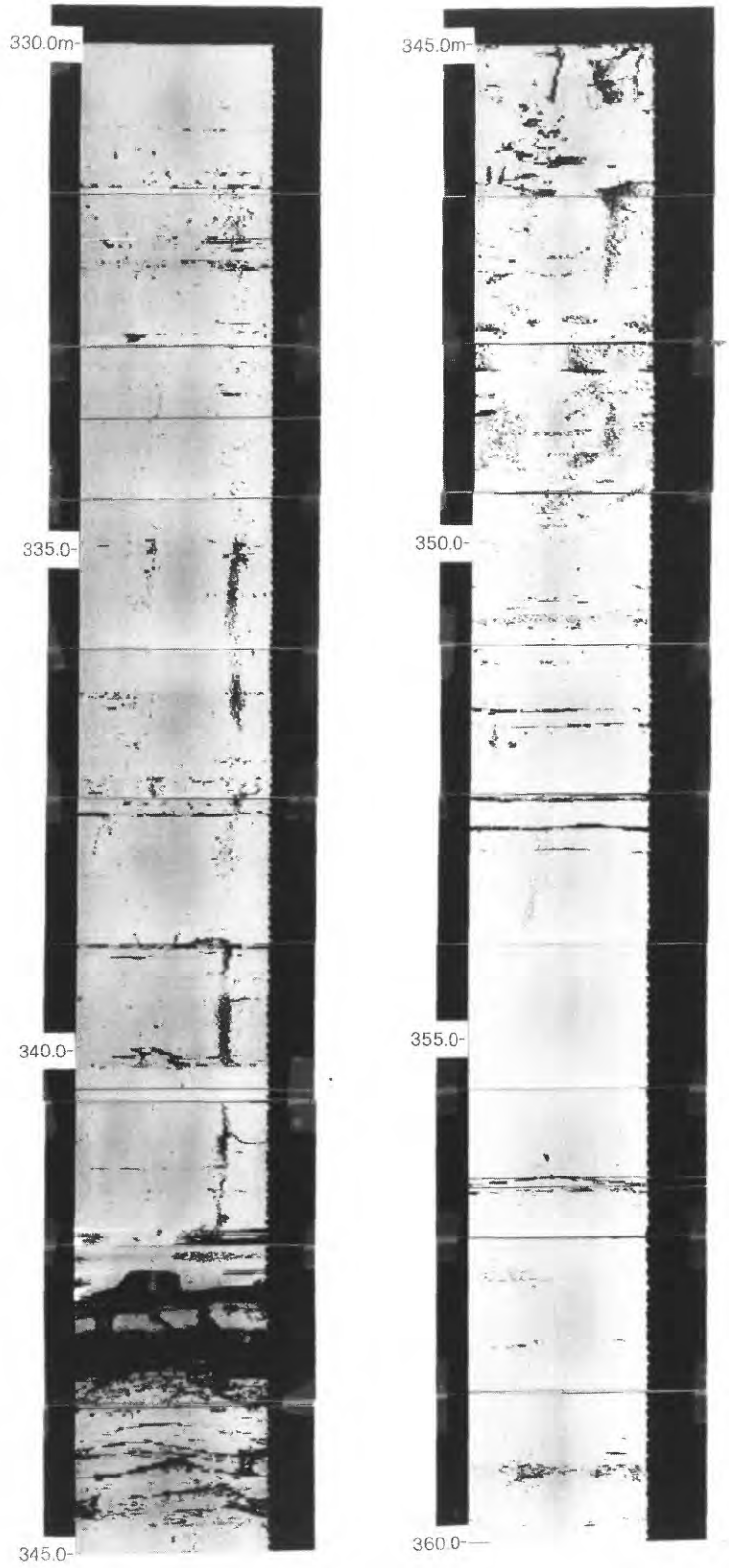
330.0m
335.0
340.0
345.0
345.0m
350.0
355.0
360.0


360.0m
365.0
370.0
375.0
375.0m
380.0
385.0
390.0

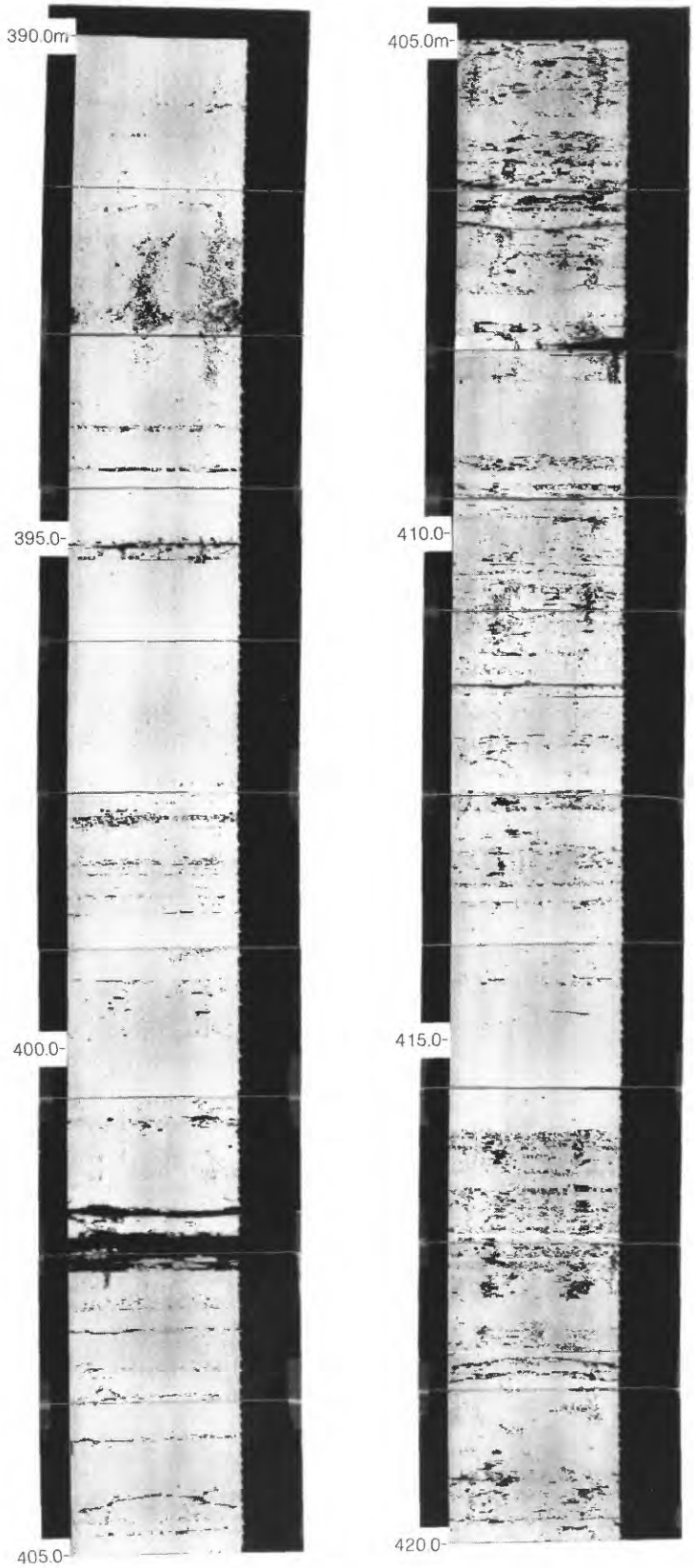
390.0m
395.0
400.0
405.0
405.0m
410.0
415.0
420.0

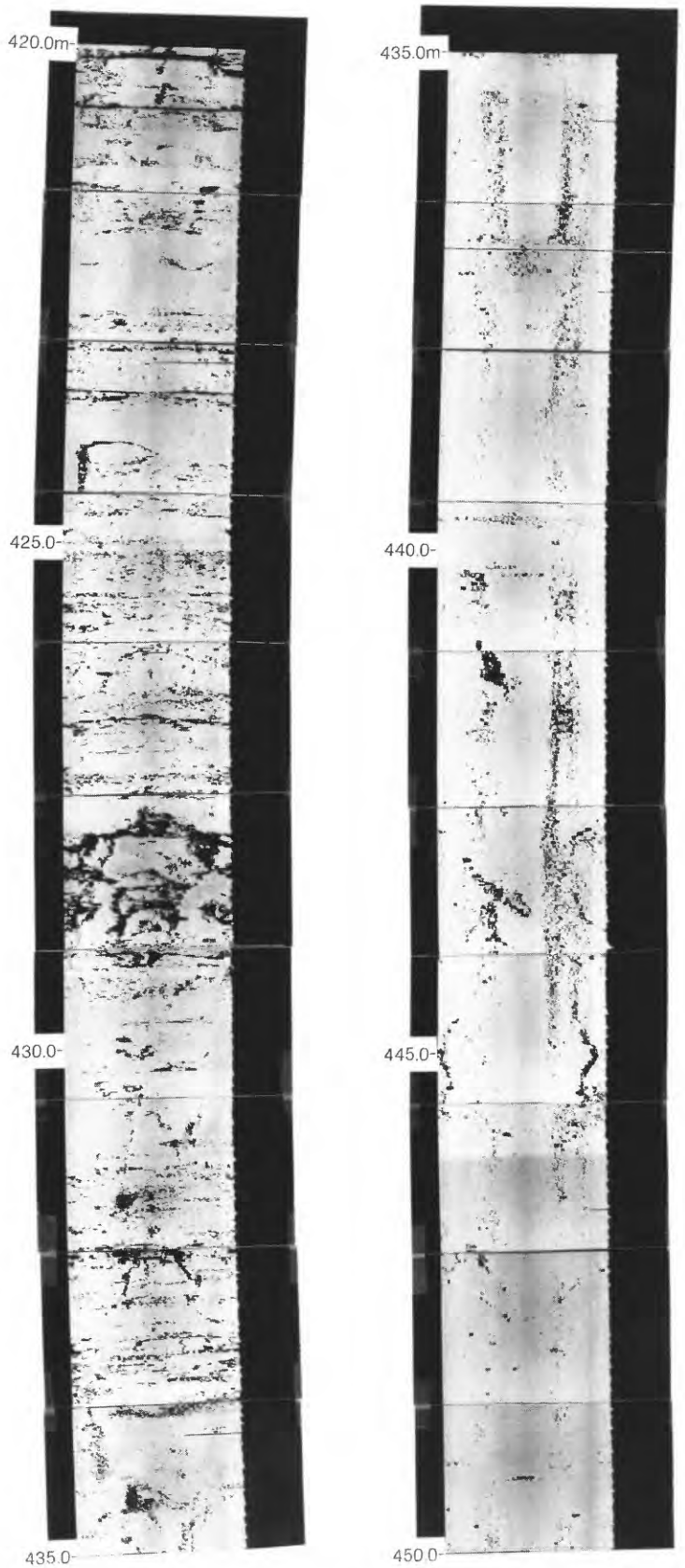
420.0m
425.0
430.0
435.0
435.0m
440.0
445.0
450.0

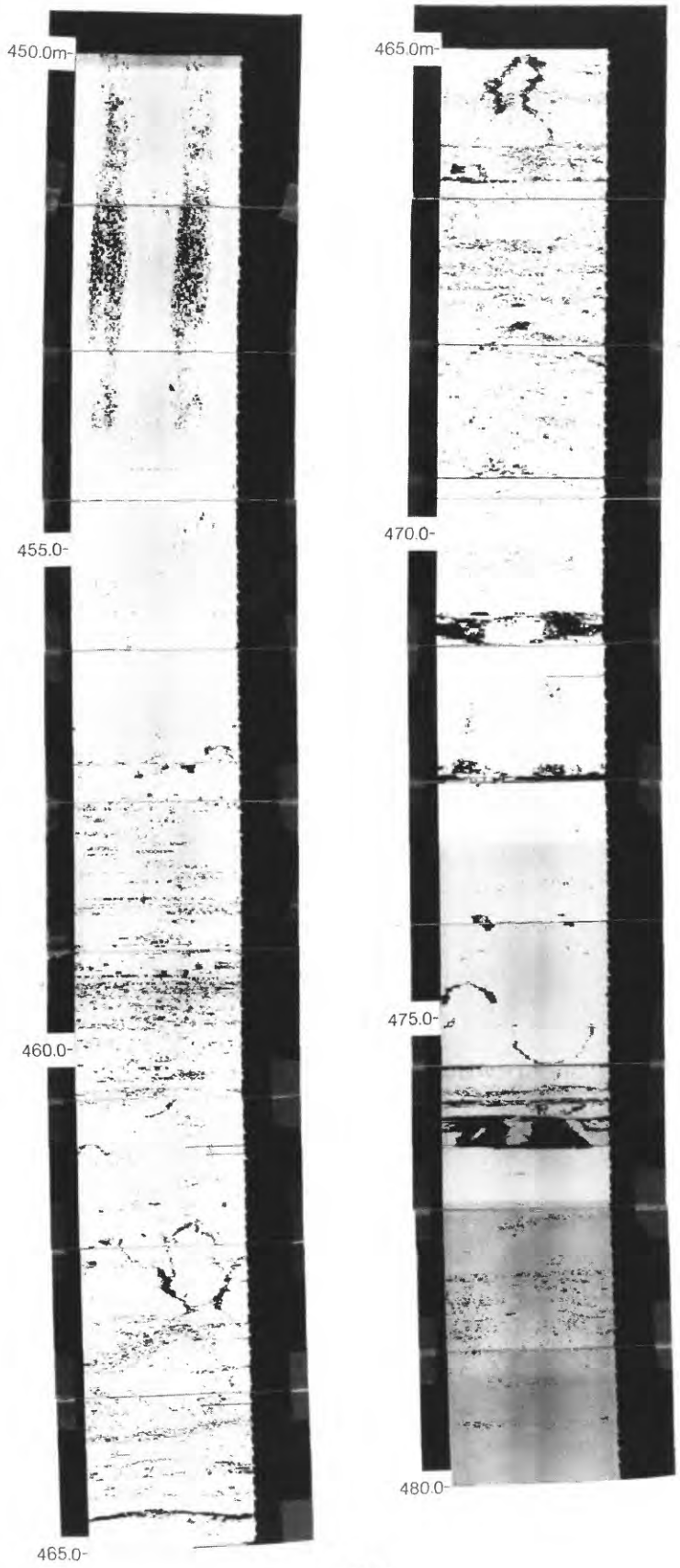
450.0m-
455.0-
460.0-
465.0-
465.0m-
470.0-
475.0-
480.0-

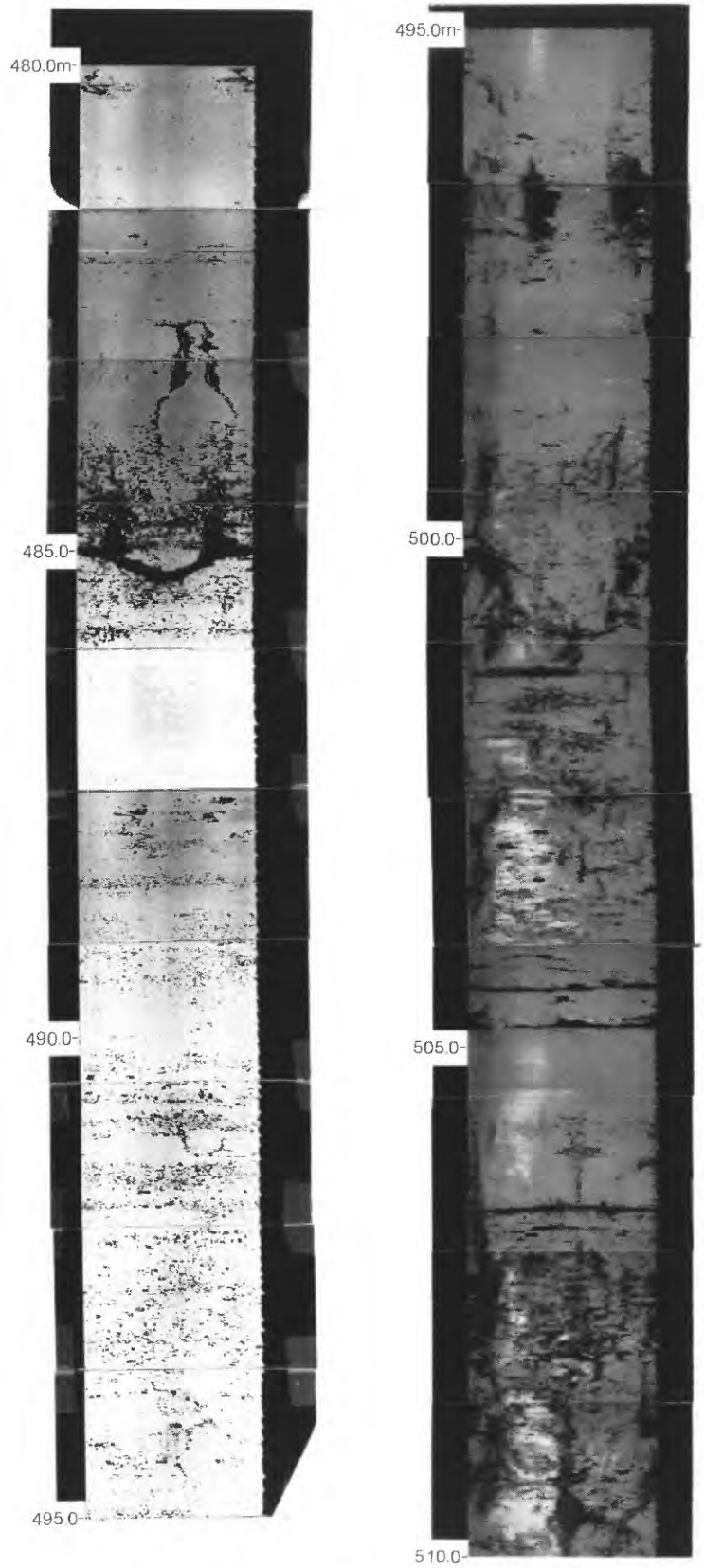
480.0m
485.0
490.0
495.0
495.0m
500.0
505.0
510.0

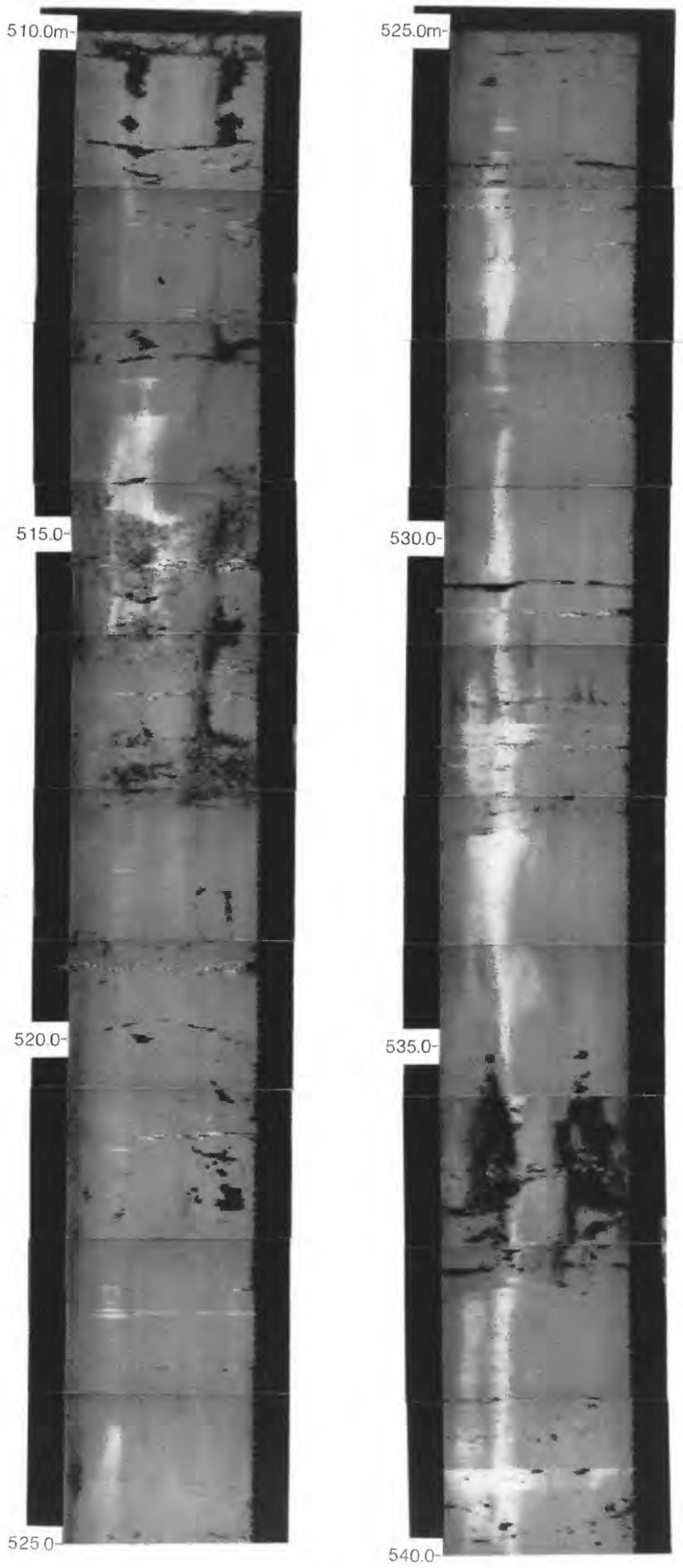
510.0m-
515.0-
520.0-
525.0-
525.0m-
530.0-
535.0-
540.0-

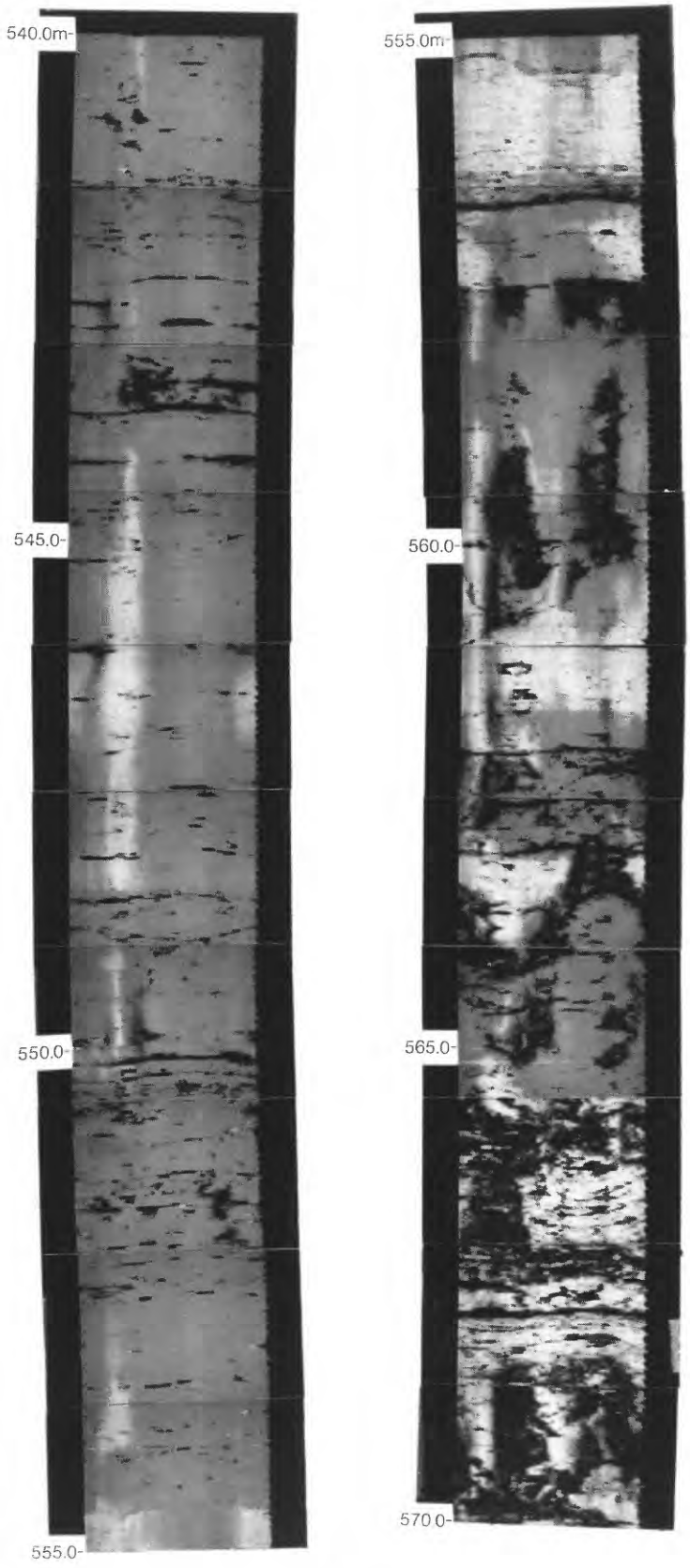
540.0m-
545.0-
550.0-
555.0-
555.0m-
560.0-
565.0-
570.0-

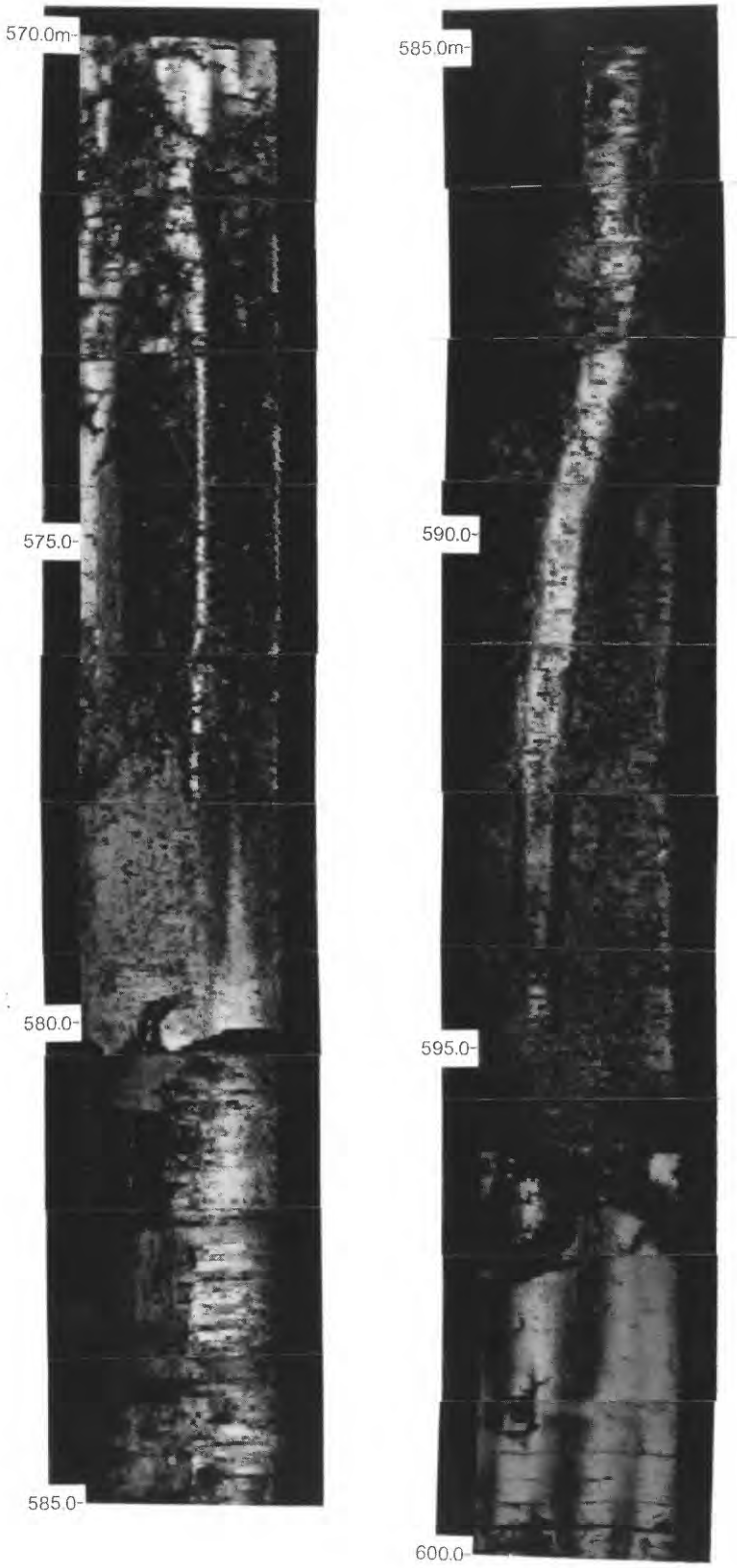
570.0m
575.0
580.0
585.0
585.0m
590.0
595.0
600.0

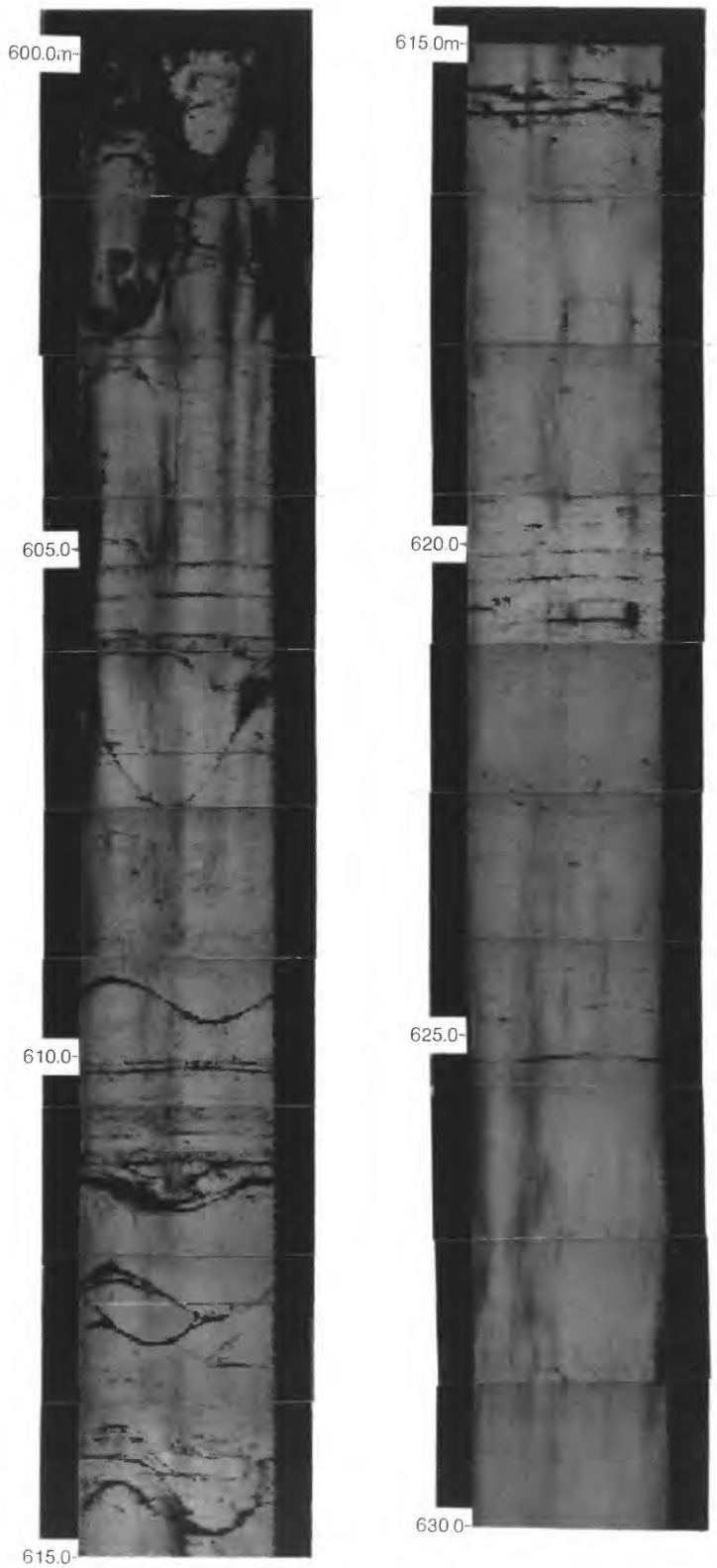
600.0m
605.0
610.0
615.0
615.0m
620.0
625.0
630.0

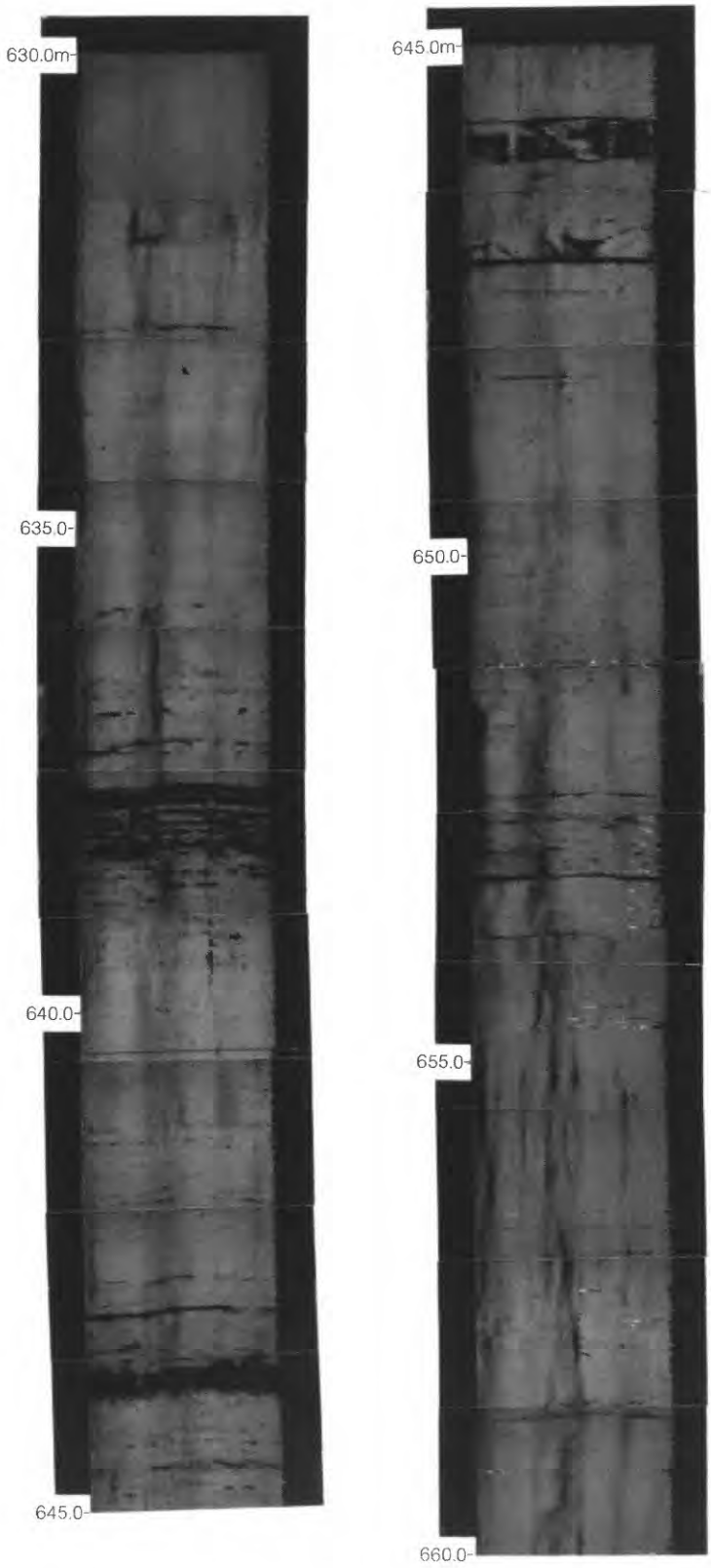
630.0m
635.0
640.0
645.0
645.0m
650.0
655.0
660.0


660.0m
665.0
670.0
675.0
675.0m
680.0
685.0
690.0

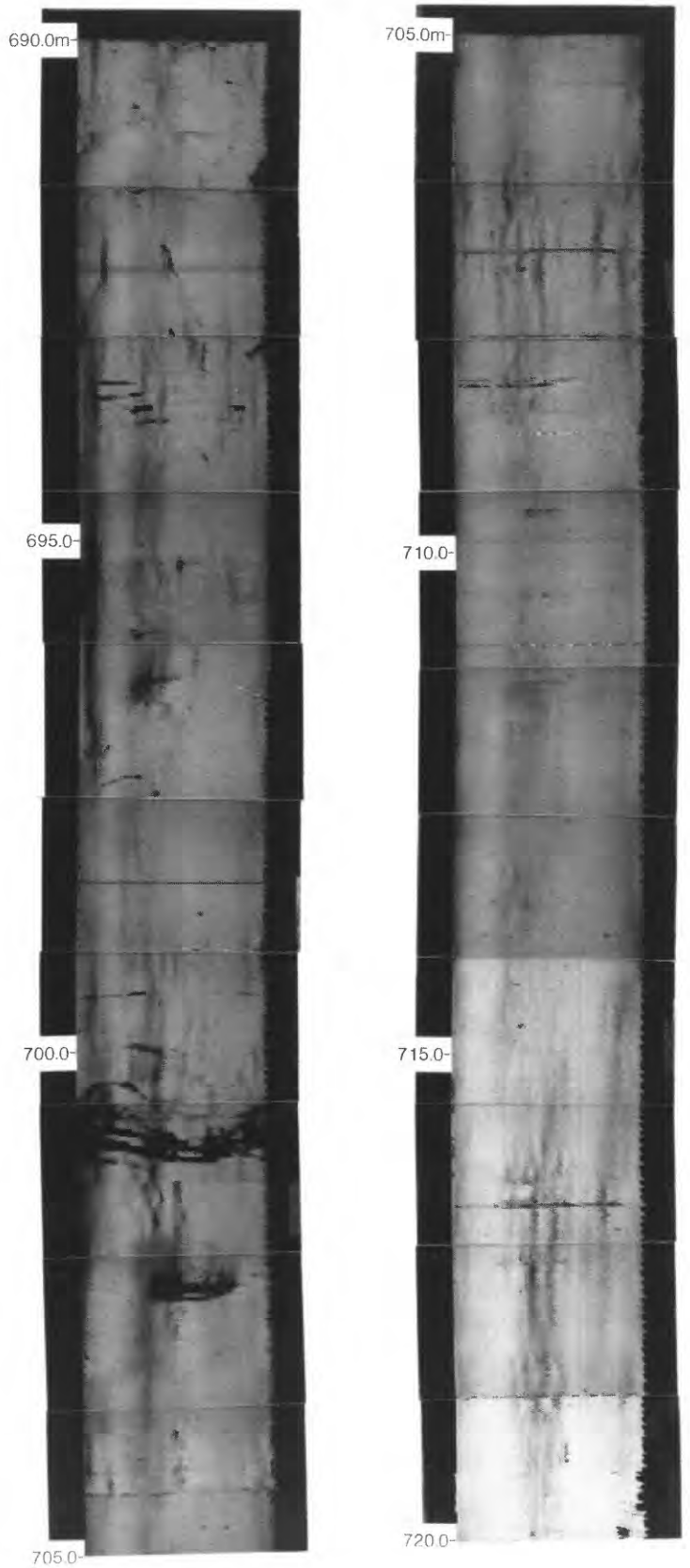
690.0m
695.0
700.0
705.0
705.0m
710.0
715.0
720.0

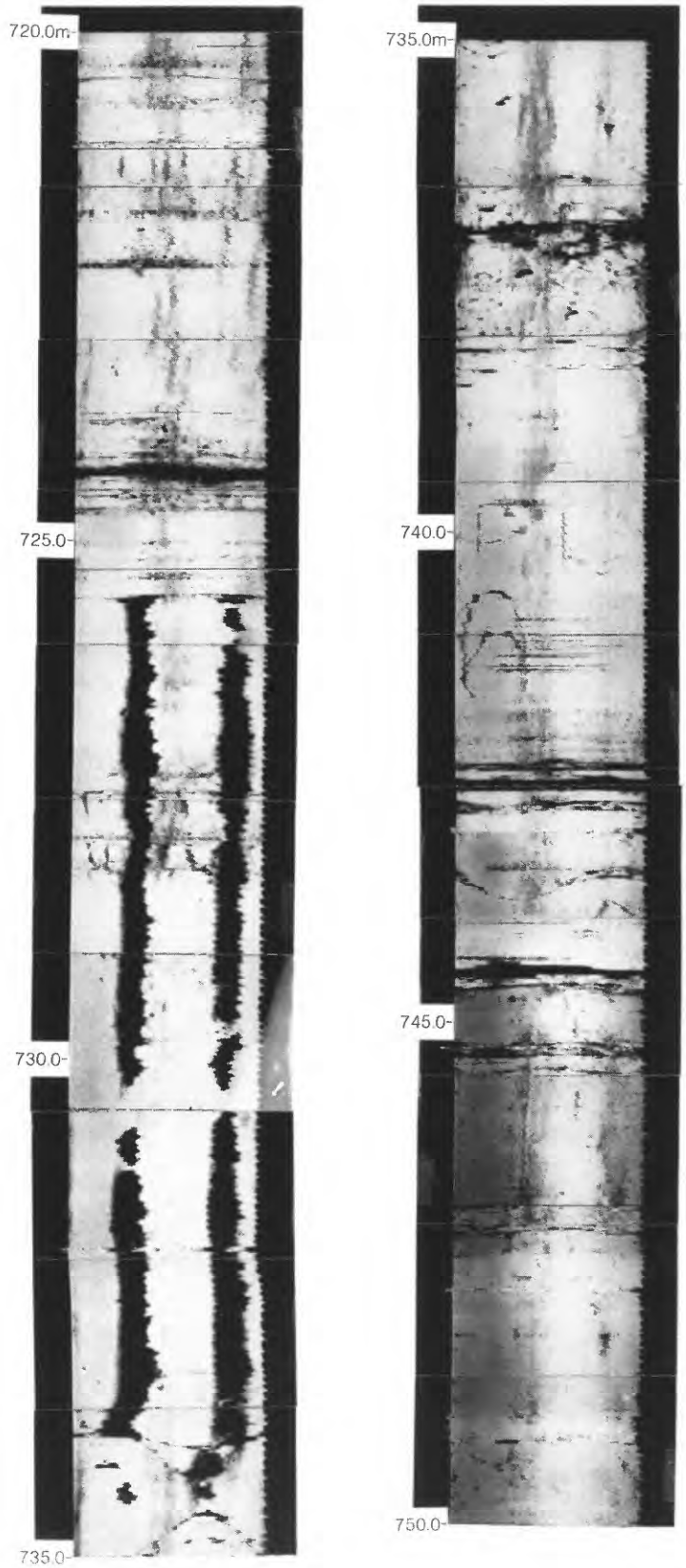
720.0m
725.0
730.0
735.0
735.0m
740.0
745.0
750.0

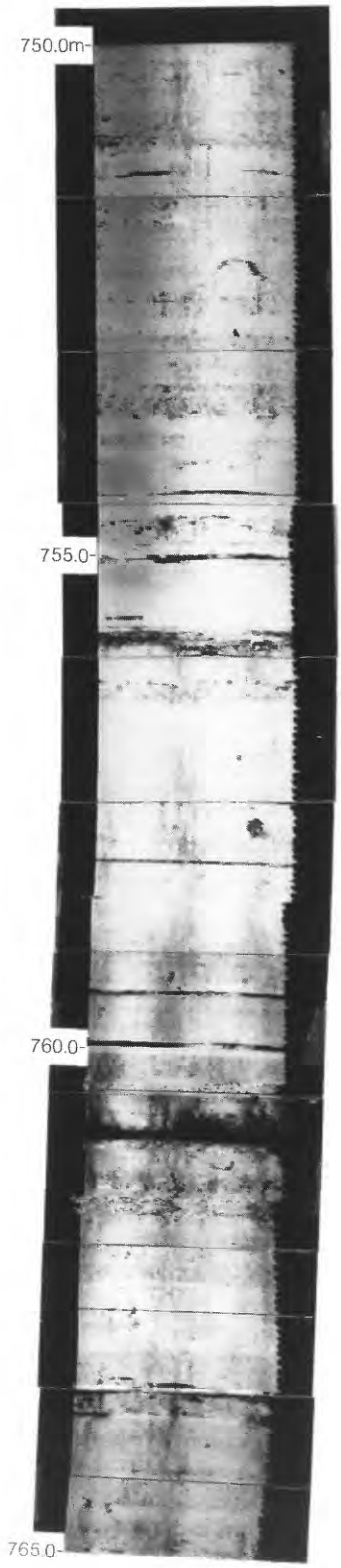
750.0m
755.0
760.0
765.0


765.0m
770.0
771.0m